© 2015. Published by The Company of Biologists Ltd | Development (2015) 142, 2203-2212 doi:10.1242/dev.119891

RESEARCH ARTICLE

Tissue-specific roles of *Fgfr2* in development of the external genitalia

Marissa L. Gredler[1], Ashley W. Seifert[1,*] and Martin J. Cohn[1,2,‡]

ABSTRACT

Congenital anomalies frequently occur in organs that undergo tubulogenesis. Hypospadias is a urethral tube defect defined by mislocalized, oversized, or multiple openings of the penile urethra. Deletion of *Fgfr2* or its ligand *Fgf10* results in severe hypospadias in mice, in which the entire urethral plate is open along the ventral side of the penis. In the genital tubercle, the embryonic precursor of the penis and clitoris, *Fgfr2* is expressed in two epithelial populations: the endodermally derived urethral epithelium and the ectodermally derived surface epithelium. Here, we investigate the tissue-specific roles of *Fgfr2* in external genital development by generating conditional deletions of *Fgfr2* in each of these cell types. Conditional deletion of *Fgfr2* results in two distinct phenotypes: endodermal *Fgfr2* deletion causes mild hypospadias and inhibits maturation of a complex urethral epithelium, whereas loss of ectodermal *Fgfr2* results in severe hypospadias and absence of the ventral prepuce. Although these cell type-specific mutants exhibit distinctive genital anomalies, cellular analysis reveals that *Fgfr2* regulates epithelial maturation and cell cycle progression in the urethral endoderm and in the surface ectoderm. The unexpected finding that ectodermal deletion of *Fgfr2* results in the most severe hypospadias highlights a major role for *Fgfr2* in the developing genital surface epithelium, where epithelial maturation is required for maintenance of a closed urethral tube. These results demonstrate that urethral tubulogenesis, prepuce morphogenesis, and sexually dimorphic patterning of the lower urethra are controlled by discrete regions of *Fgfr2* activity.

KEY WORDS: Fgf, Genitalia, Mouse, Sexual differentiation, Tubulogenesis, Urethra

INTRODUCTION

Tubular morphogenesis (tubulogenesis) is essential for normal embryonic development, and organs that undergo tubulogenesis are frequently affected by congenital anomalies (Ray and Niswander, 2012). A variety of mechanisms can drive tube formation, such as the wrapping mechanism of neurulation, budding of the salivary and mammary glands, and the delamination/migration process of bile duct development (Andrew and Ewald, 2010; Caviglia and Luschnig, 2014; Luschnig and Uv, 2014; Zegers, 2014). Hypospadias, a urethral tube defect defined by a mislocalized urethral opening (meatus), is among the most common birth defects in humans, affecting ~1 in 250 live births (Paulozzi et al., 1997; Baskin et al., 2001).

[1]Department of Biology, UF Genetics Institute, University of Florida, PO Box 103610, Gainesville, FL 32611, USA. [2]Howard Hughes Medical Institute, Department of Molecular Genetics and Microbiology, University of Florida, PO Box 103610, Gainesville, FL 32611, USA.
*Present address: University of Kentucky, Department of Biology, 211 TH Morgan Building, Lexington, KY 40506-0225, USA.

‡Author for correspondence (mjcohn@ufl.edu)

Received 13 November 2014; Accepted 5 May 2015

External genital development involves a series of budding and fusion events. Paired genital swellings arise lateral to the cloacal membrane, around embryonic day (E) 10.5 in the mouse, and these swellings then merge to form a single genital tubercle by E11.5 (Perriton et al., 2002). By E13.5, paired preputial swellings have emerged from the lateral margins at the base of the genital tubercle and eventually give rise to the prepuce (foreskin and clitoral hood; Perriton et al., 2002). At E14.5, the labioscrotal swellings protrude caudally and later will either fuse to form the male scrotum or will remain unfused to form the female labia majora (Perriton et al., 2002). After the monomorphic phase of external genital patterning, which lasts until ~E15, sexually dimorphic patterning is regulated by sex hormones synthesized by the testes and ovaries.

The embryonic urethra develops via the inclusion of cloacal endoderm in the nascent genital tubercle (Perriton et al., 2002; Seifert et al., 2008), where it persists as a bilaminar epithelial plate through E14, when it begins to cavitate from proximal to distal to form the lumen of the urethral tube (Perriton et al., 2002; Cohn, 2011). In males, invasion of the urorectal septum mesenchyme into the genital tubercle displaces the urethral tube to a central position within the penis, whereas in females, the endoderm remains tethered to the ventral side of the glans (Glenister, 1954; Seifert et al., 2008). Thus, urethral tubulogenesis involves multiple morphogenetic processes, including evagination of the cloacal wall to form the bilaminar plate, epithelial stratification and maturation, and remodeling of the plate to form the lumen of the tube.

A number of studies have reported that the incidence of hypospadias and other defects of the external genitalia (such as cryptorchidism and chordee) has increased over the past several decades (Paulozzi et al., 1997; Toppari et al., 2010; Nordenvall et al., 2014). Although most instances of hypospadias are idiopathic (Van der Zanden et al., 2012), molecular genetic analyses of affected individuals have revealed nucleotide variants (Tannour-Louet et al., 2010, 2014; Geller et al., 2014), epigenetic anomalies (Vottero et al., 2011), protein modifications (Qiao et al., 2011), and mutations in known developmental genes (Beleza-Meireles et al., 2007; Carmichael et al., 2013). The results of genetic, toxicological, and epidemiological studies have led to the proposal that urethral tube defects are caused by the combinatorial effects of aberrant hormone activity, such as that caused by exposure to environmental endocrine-disrupting compounds (Michalakis et al., 2014; Winston et al., 2014), and underlying genetic susceptibility (Wang and Baskin, 2008; Kalfa et al., 2009, 2011; Toppari et al., 2010; Yiee and Baskin, 2010; Van der Zanden et al., 2012).

We previously reported that deletion of either *Fgf10* or its receptor *Fgfr2iiib* (the epithelial isoform of *Fgfr2*) results in severe hypospadias (Petiot et al., 2005). *Fgf10* is expressed in the genital mesenchyme, and *Fgfr2* is transcribed in the adjacent urethral epithelium and in the surface ectoderm (Haraguchi et al., 2000; Satoh et al., 2004; Petiot et al., 2005; Ching et al., 2014). *Fgfr2iiib*$^{-/-}$ mice develop hypospadias associated with decreased proliferation

Development (2015) 142, 2203-2212 doi:10.1242/dev.119891

and stratification of urethral cells that results from failure to maintain the progenitor cell layer of the urethral epithelium (Petiot et al., 2005). Importantly, *Fgfr2* transcription in the genital tubercle can be downregulated by exposure to the androgen receptor (AR) antagonist flutamide in a dose-dependent manner (Petiot et al., 2005), suggesting that *Fgfr2* acts as a link between hormonal and genetic regulation of external genital development.

The complex expression pattern of *Fgfr2iiib* and the compound phenotype of *Fgfr2iiib*$^{-/-}$ mice precluded a determination of the tissue-specific roles of *Fgfr2*. To determine which domain(s) of *Fgfr2* expression regulate(s) urethral tubulogenesis, we generated conditional mutants in which *Fgfr2* is deleted from either the urethral endoderm or the surface ectoderm. Conditional deletion of *Fgfr2* results in two distinct phenotypes: endodermal *Fgfr2* ablation causes mild hypospadias and inhibits maturation of a complex urethral epithelium, whereas loss of ectodermal *Fgfr2* induces severe hypospadias and failure of ventral prepuce closure. Although these compartment-specific mutants exhibit distinctive genital anomalies, we find that at the cellular level, *Fgfr2* plays similar roles in the urethral tube and surface ectoderm. These results demonstrate that urethral tubulogenesis, prepuce morphogenesis, and sexually dimorphic patterning of the urethra are three crucial processes in external genital development that are controlled by independent regions of *Fgfr2* activity.

RESULTS

Distinct regions of *Fgfr2* signaling mediate development of the prepuce and urethra

To dissect the roles of the urethral endodermal and the surface ectodermal domains of *Fgfr2* in external genital development, we performed conditional deletions of *Fgfr2*^{flox} using the *Shh*^{gfpcre} and *Msx2*^{cre} alleles (Sun et al., 2000; Yu et al., 2003; Harfe et al., 2004). *Fgfr2* was ablated in urethral endoderm in *Shh*$^{gfpcre/+}$; *Fgfr2*$^{flox/flox}$ mice, which will be referred to as *Fgfr2*$^{Endo\Delta}$ mutants. The ectodermal domain of *Fgfr2* was deleted in *Msx2*-Cre; *Fgfr2*$^{flox/flox}$ mice, which will be referred to as *Fgfr2*$^{Ecto\Delta}$ mutants. Removal of *Fgfr2* from target tissues was verified by whole-mount *in situ* hybridization using a riboprobe that detects the floxed region of *Fgfr2* (supplementary material Fig. S1). To examine whether *Fgfr2* deletion in one epithelial population affects *Fgfr2* signaling in another region, we used immunofluorescence for FGFR2. We found no changes in the localization of ectodermal FGFR2 in *Fgfr2*$^{Endo\Delta}$ mutants, of urethral FGFR2 in *Fgfr2*$^{Ecto\Delta}$ mutants or of mesenchymal FGFR2 in either mutant (supplementary material Fig. S1), indicating that *Fgfr2* conditional deletion from the urethra does not affect ectodermal *Fgfr2* signaling and vice versa.

To facilitate identification of *Fgfr2*$^{\Delta}$ cells, we used the *Rosa26*^{lacZ} reporter (R26R; Soriano, 1999) and fate-mapped Cre-expressing lineages with X-Gal staining. In control (*Shh*$^{gfpcre/+}$, *R26R*) male genitalia at postnatal day (P) 0, *lacZ*$^{+}$ cells are present in three locations: the urethral epithelium, the perineal raphe, and the preputial glands (Fig. 1A; Seifert et al., 2008). External genitalia of male *Fgfr2*$^{Endo\Delta}$ mutants at P0 appeared generally normal (the prepuce enveloped the glans and was fused at the ventral midline); however, lineage tracing revealed that ectopic endodermal cells were exposed on the ventral surface of the penis and a distal urethral meatus was absent (Fig. 1B). The stripe of endodermally derived cells along the perineum was thinner mediolaterally, shorter anteroposteriorly and had an irregular border relative to controls (Fig. 1B). The intermingling of urethral endodermal and surface ectodermal cells suggests a relaxation of the boundary between these cell populations (Fig. 1B). These results indicate that in males, deletion of *Fgfr2* in the endoderm results in incomplete internalization of urethral epithelial cells.

Fgfr2$^{Ecto\Delta}$ mutants developed hypospadias with a range of severity. In male mutants with the most extensive hypospadias, preputial ectodermal cells failed to fuse along the ventral margin of the penis, resulting in complete exposure of the (*lacZ*$^{-}$) urethral plate (Fig. 1D), whereas mutants with localized ectopic urethral openings were characterized by partial fusion of the prepuce around the urethral plate (supplementary material Fig. S2). Mosaicism in *Msx2*^{cre} activity was visible by discontinuous distribution of *lacZ*$^{+}$ cells in both mutant and control embryos (Fig. 1C,D; supplementary material Fig. S2). These data show that deletion of ectodermal *Fgfr2* results in penile hypospadias, indicating that *Fgfr2* activity in the surface epithelium is required for morphogenesis of the ventral prepuce and enclosure of the urethral tube.

Both male and female *Fgfr2* null mutants were reported to develop hypospadias (Petiot et al., 2005). During normal development, newborn male and female external genitalia show clear dimorphism; females display a more proximal urethral meatus, a vaginal opening at the base of the glans, a broad domain of endodermally derived cells in the perineal raphe and a short anogenital distance (Fig. 1E,G). *Fgfr2*$^{Endo\Delta}$ mutant females at P0 had a hypoplastic vaginal opening in which *lacZ*$^{+}$ cells extended both laterally onto the surface of the perineum and distally onto the clitoral skin (Fig. 1F). This was reminiscent of the mislocalized endodermal cells at the base of the glans in *Fgfr2*$^{Endo\Delta}$ mutant males. An additional similarity with *Fgfr2*$^{Endo\Delta}$ males was that the population of *lacZ*$^{+}$ endodermally derived cells along the perineal raphe was thinner and shorter than in controls (Fig. 1F). The urethral meatus of control females was visible at the apex of the prepuce,

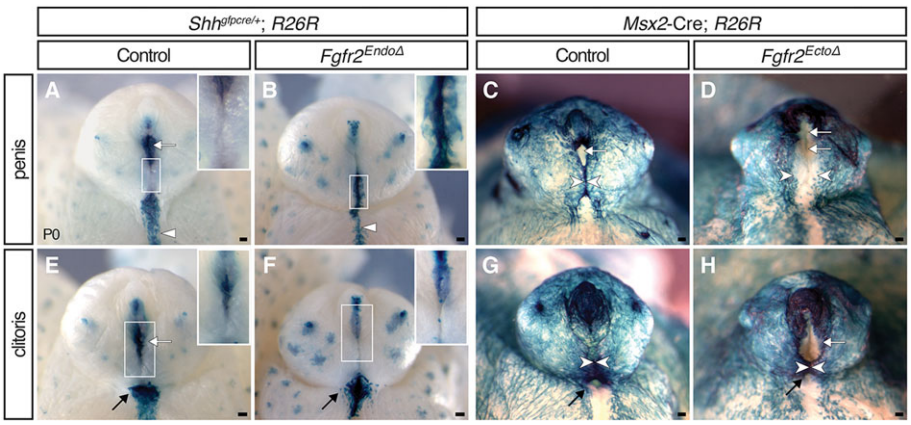

Fig. 1. External genital morphologies and mutant cell fates in *Fgfr2* conditional knockout mice. (A,B,E,F) Endoderm fate-mapping in *Shh*$^{gfpcre/+}$; *R26R* mice demonstrates that *Fgfr2*$^{Endo\Delta}$ males have an irregular perineal raphe (triangles) and females have a dysmorphic vaginal opening (black arrows). Both sexes have ectopic endodermal cells on the preputial skin (inset) and lack a distal urethral meatus (white arrows). (C,D,G,H) Ectoderm fate-mapping in *Msx2*-Cre; *R26R* mice reveals failed prepuce closure (white arrowheads) in *Fgfr2*$^{Ecto\Delta}$ males and severe hypospadias in *Fgfr2*$^{Ecto\Delta}$ males and females. Scale bars: 100 µm.

Development (2015) 142, 2203-2212 doi:10.1242/dev.119891

where the lateral preputial folds abut the glans (Fig. 1E). This region was absent from *Fgfr2*^{EndoΔ} clitorises, and ectopic punctate domains of *lacZ*$^{+}$ endodermal cells were visible along the ventral midline (Fig. 1F, inset). Thus, the external genitalia of newborn male and female *Fgfr2*^{EndoΔ} mutants have endodermally derived cells ectopically positioned in the surface epithelium of the prepuce, and an irregular boundary of endodermal and ectodermal cells along the perineal raphe.

Female *Fgfr2*^{EctoΔ} mutants had hypospadias with a range of severities similar to those observed in males. In female *Fgfr2*^{EctoΔ} mutants with severe hypospadias, the prepuce was completely unfused, resulting in a single urogenital opening (supplementary material Fig. S2). A subset of neonatal female *Fgfr2*^{EctoΔ} mutants had a large, proximally displaced (hypospadic) urethral meatus and a partially fused prepuce that separated the tip of the urethral plate from the vaginal orifice (Fig. 1H; supplementary material Fig. S2). Thus, ectodermal *Fgfr2* deletion causes severe hypospadias and perturbs prepuce morphogenesis in both sexes.

Fgfr2 conditional deletions disrupt urethral internalization and cause hypospadias

Histological analysis provided further insight into the external genital anomalies of *Fgfr2* conditional mutants. In transverse sections through the distal penis of newborn control mice, the left and right sides of the prepuce fused ventrally, dividing the endodermal epithelium into a urethral tube dorsally and the penile raphe ventrally (Fig. 2A,C,E,G). In sections through this region of *Fgfr2*^{EndoΔ} mutant males, the urethral epithelium was not septated into a dorsal tube and ventral seam, but instead persisted as a urethral plate that extended from the center of the tubercle to the ventral margin, similar to the morphology seen in the control female clitoris (compare mutant penis in Fig. 2J with control penis in 2I and control clitoris in 2U). The distal penis of *Fgfr2*^{EctoΔ} males displayed an unfused prepuce and an open urethral sulcus (Fig. 2D,H). Within the penile shaft of controls, the urethral tube was positioned at the ventral margin of the glans, which was completely enveloped by the prepuce (Fig. 2I,K). By contrast, the urethral epithelium of both *Fgfr2*^{EndoΔ} and *Fgfr2*^{EctoΔ} mutants extended ventrally from the glans through the unfused prepuce and was contiguous with the ventral surface ectoderm, resulting in hypospadias (Fig. 2F). In control and *Fgfr2*^{EndoΔ} females, the distal urethra formed a solid epithelial cord that lacked a lumen (Fig. 2Q,R), whereas the proximal urethra was an open tube that remained attached to the ventral ectoderm (Fig. 2U,V). In *Fgfr2*^{EctoΔ} females, the ventral margin of the urethral plate developed an open, hypospadic phenotype along the proximodistal axis of the clitoris (Fig. 2, compare enclosed tube in S,W with open groove in T,X). These data indicate that, in males, both endodermal and ectodermal *Fgfr2* deletions interrupt urethral internalization, endodermal *Fgfr2* deletion disrupts urethral canalization, and ectodermal *Fgfr2* deletion disrupts fusion of the ventral prepuce and urethral internalization. In females, only ectodermal *Fgfr2* deletion results in hypospadias with an open ventral prepuce proximally.

Endodermal *Fgfr2* regulates maturation of a complex urethral epithelium

To identify the cellular basis of hypospadias in mice lacking urethral *Fgfr2*, we examined *Fgfr2*^{EndoΔ} and control genital tubercles at E14.5 by scanning electron microscopy (SEM), histology, fate mapping and immunohistochemistry. At E14.5, *Fgfr2*^{EndoΔ} mutant external genitalia were morphologically similar to controls; each had developed a genital tubercle with a urethral seam along the ventral midline and preputial swellings on the lateral margins, labioscrotal swellings on the ventral body wall just below the preputial swellings, and a proximal urethral opening located at the base of the tubercle (Fig. 3A,B). At high magnification, the proximal urethral opening of control embryos was oval-shaped, in contrast to the diamond-shaped opening of *Fgfr2*^{EndoΔ} mutants (Fig. 3C,D). Given that *Fgfr2* was deleted only in the endoderm, we hypothesized that this malformation of the proximal urethra is a direct consequence of morphogenetic changes in the urethral epithelium. By histological analysis, three features of urethral

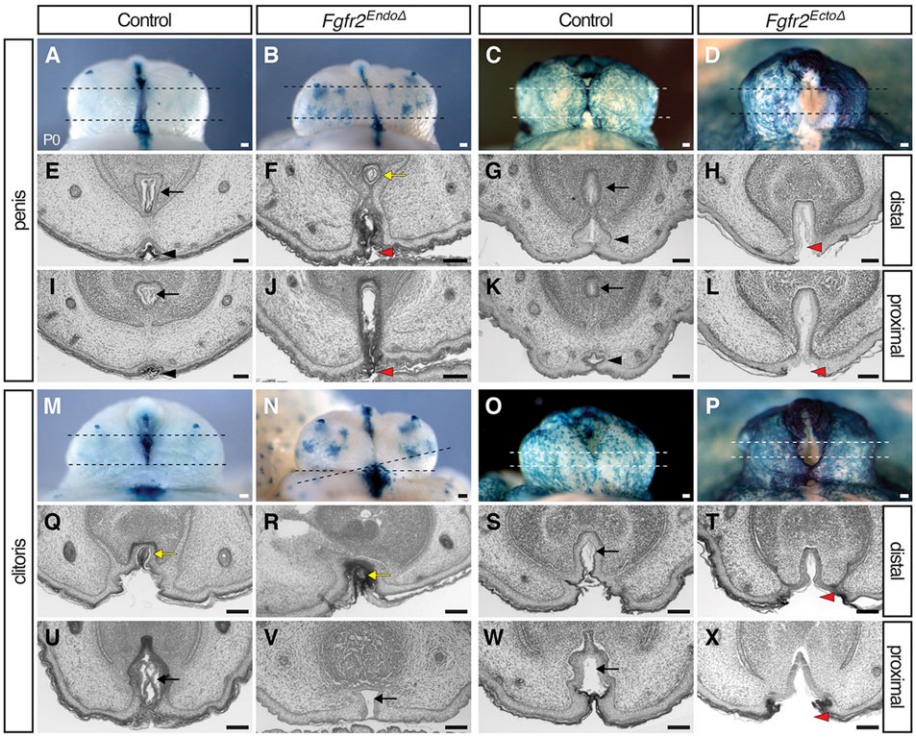

Fig. 2. Urethral morphology in newborn males and females with conditional deletions of *Fgfr2*. Lineage tracing (A-D,M-P) and histological sections (E-L,Q-X) of the external genitalia in newborn male (A-L) and female (M-X) *Fgfr2* conditional mutants. Urethral internalization is disrupted in *Fgfr2*^{EndoΔ} (F,J) and *Fgfr2*^{EctoΔ} (H,L) males. *Fgfr2*^{EctoΔ} males (H,L) and females (T,X) develop severe hypospadias. Dashed lines in A-D and M-P indicate planes of section in E-L and Q-X, respectively. Black arrows mark the internal urethral tube, black triangles indicate the penile raphe, yellow arrows denote an endodermal epithelial cord, and red triangles mark hypospadic urethral openings. Histological images were converted to grayscale using Adobe Photoshop. Scale bars: 100 µm.

Development (2015) 142, 2203-2212 doi:10.1242/dev.119891

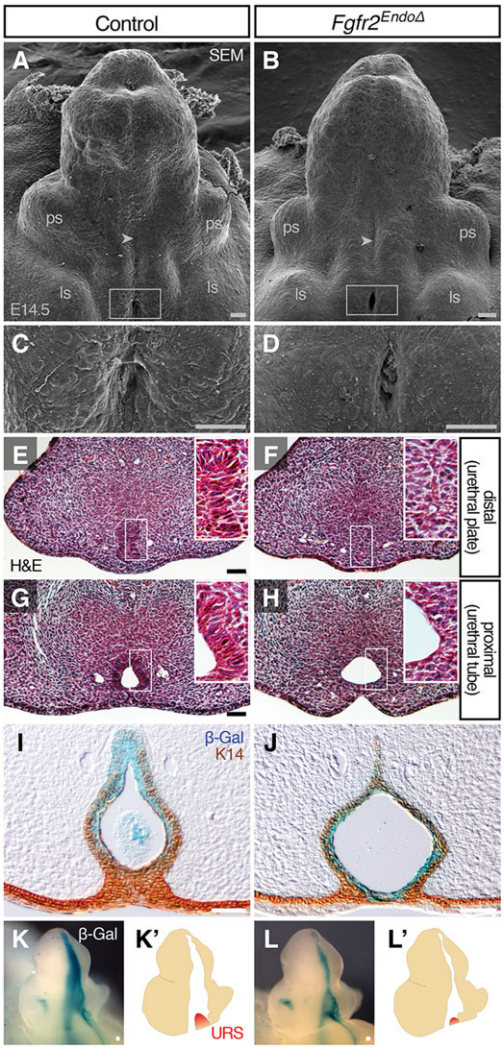

Fig. 3. Development of the genital tubercle and urethral epithelium in the absence of endodermal *Fgfr2*. (A-D) SEM analysis shows that *Fgfr2*^{EndoΔ} mutants develop abnormal proximal urethral openings (C and D are higher magnification views of boxes in A and B, respectively), but properly patterned preputial swellings (ps), labioscrotal swellings (ls) and urethral seams (arrowheads). (E-H) Histological sections of mutant and control genital tubercles show that the proximal urethra (G,H) forms a urethral lumen, whereas the distal urethra (E,F) remains a bilaminar plate at E14.5. (I,J) Immunohistochemical analysis of K14 on β-Gal-stained sections reveals a thin urethral epithelium in *Fgfr2*^{EndoΔ} mutants and absence of EMT. (K-L′) Whole-mount X-Gal-staining of β-Gal-expressing endoderm at E14.5 shows reduction of urorectal septum (URS) invasion into *Fgfr2*^{EndoΔ} mutant genital tubercle relative to controls. Scale bars: 50 µm.

morphogenesis were evident in E14.5 control embryos: the proximal penile urethra contained an open lumen, the distal urethra was a bilaminar epithelial plate, and a complex, stratified epithelium was evident along the proximodistal axis of the urethra (Fig. 3E,G; Perriton et al., 2002). In controls and *Fgfr2*^{EndoΔ} mutants, a urethral lumen was apparent in the proximal urethra while a closed urethral plate persisted distally; however, in *Fgfr2*^{EndoΔ} mutants the urethral epithelium appeared thinner and less stratified (Fig. 3F,H). The finding that *Fgfr2*^{EndoΔ} mutant urethrae show diminished stratification indicates that *Fgfr2* is required for the endoderm to mature into a complex epithelium.

Previous studies of *Fgfr2iiib* knockout mice suggested that, between E13.5 and E15.5, the loss of the tubular urethra could be the result of an epithelial-mesenchymal transition (EMT) (Petiot et al., 2005). To test for the presence of endodermal cells in the genital mesenchyme, we sectioned β-galactosidase-stained *Fgfr2*^{EndoΔ} and control genital tubercles and labeled epithelial cells with an antibody against cytokeratin 14 (K14), an intermediate filament produced in the genital epithelium but not in the mesenchyme (Kurzrock et al., 1999). In both mutants and controls, the margin of the K14^{+} urethral epithelium also marked the boundary of *lacZ*$^{+}$ cells; blue cells were not observed in the mesenchyme (Fig. 3I,J), and this pattern persisted throughout the proximodistal length of control and mutant genital tubercles (supplementary material Fig. S3). Thus, deletion of *Fgfr2* from the urethral endoderm disrupts maturation of the urethral epithelium but does not lead to an EMT.

During normal masculinization of the urethral plate, ingrowth of the urorectal septum into the proximal genital tubercle partitions the urethral plate into a definitive urethral tube dorsally and a penile raphe ventrally (Seifert et al., 2008). In light of our finding that urethral internalization is disrupted following endodermal *Fgfr2* deletion, we investigated whether this process is disrupted in *Fgfr2*^{EndoΔ} mutants. At E14.5, migration of the urorectal septum into the proximal genital tubercle was evident in control males (Fig. 3K,K′). Urorectal septum mesenchyme also was detectable at the base of the genital tubercle in *Fgfr2*^{EndoΔ} mutants, although it did not extend into the genital tubercle as in controls (Fig. 3L,L′). These data are consistent with our finding that the glanular urethral tube is absent from male *Fgfr2*^{EndoΔ} mutants at birth.

Ectodermal *Fgfr2* is required for preputial development and urethral morphogenesis

We next investigated ontogeny of the hypospadias resulting from ectodermal *Fgfr2* deletion by examining *Fgfr2*^{EctoΔ} genital tubercles using SEM. In control mice at E14.5, the preputial swellings had begun to grow ventromedially (Fig. 4A). In *Fgfr2*^{EctoΔ} mutants, the preputial swellings were positioned lateral and slightly dorsal to the developing glans, and the proximal urethral opening was both wider mediolaterally and extended farther proximodistally compared with controls (Fig. 4C, compare with B and D). Within the larger urethral orifice of *Fgfr2*^{EctoΔ} mutants, the exposed cells were stretched across the urethral seam, indicative of mechanical tension across the ventral midline of the tubercle (Fig. 4D). Mislocalization of the preputial swellings was evident from the onset of prepuce development (E13.0) and occurred in conjunction with urethral abnormalities that progressed from supernumerary urethral openings at E13 to hypospadic orifices at later stages (supplementary material Fig. S4). These results indicate that removal of *Fgfr2* from the genital tubercle ectoderm disrupts ventral growth of the prepuce.

We next investigated the possibility that the abnormal urethral opening and mislocalized preputial swellings of *Fgfr2*^{EctoΔ} mutants might be associated with urethral tube defects internally. Analysis of transverse histological sections showed that the dorsal urethra of controls and *Fgfr2*^{EctoΔ} mutants at E14.5 was a solid, bilaminar plate along the proximodistal axis of the genital tubercle, whereas the ventral urethra had opened into a lumen proximally and retained bilaminar morphology distally (Fig. 4E-H). However, in *Fgfr2*^{EctoΔ} mutants, the ventral side of the urethral epithelium formed an open groove (sulcus) rather than a tube, exposing the underlying urethral plate such that it was visible on the surface of the genital tubercle (Fig. 4D,H). In coronal sections, the urethral tube of controls had a teardrop-shaped or cylindrical morphology that decreased in size from

Development (2015) 142, 2203-2212 doi:10.1242/dev.119891

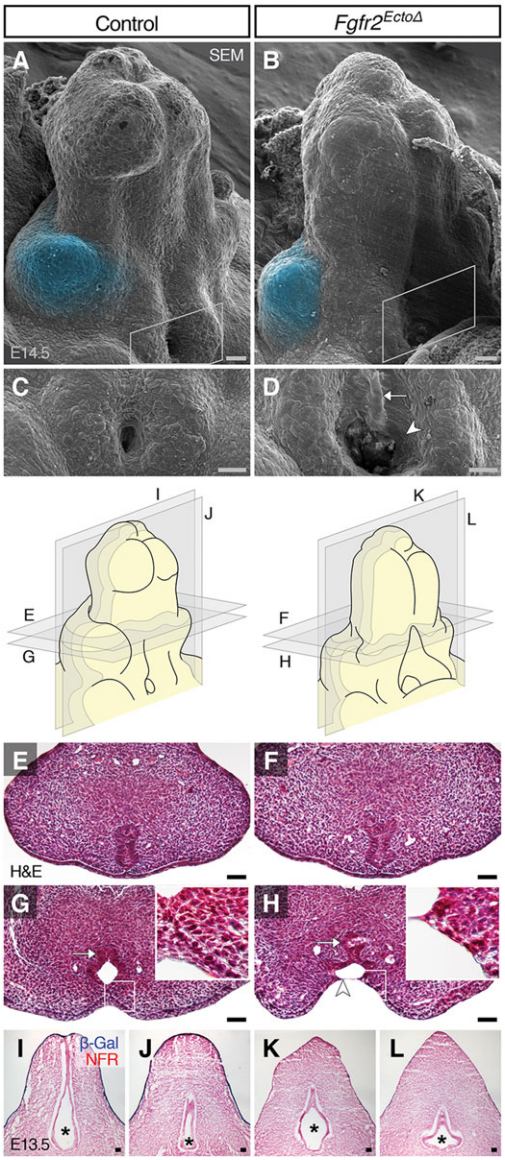

Fig. 4. Effects of ectodermal *Fgfr2* deletion on dorsoventral preputial swelling position and urethral lumen morphology. (A-D) SEM shows that E14.5 $Fgfr2^{Ecto\Delta}$ mutants have dorsally displaced preputial swellings (blue pseudocolor) with an enlarged proximal urethral opening (white boxes in A and B, shown at higher magnification in C and D, respectively). Note the stretched urethral cells (arrowhead) and the exposed urethral plate (arrow) in $Fgfr2^{Ecto\Delta}$ mutants (D). (E-H) Histological cross-sections (cut perpendicular to the long axis of the GT) show a bilaminar plate in the distal urethra of both mutants and controls at E14.5. Proximally, $Fgfr2^{Ecto\Delta}$ mutant urethral epithelium maintains a normal bilaminar plate arrangement in the dorsal urethra (arrow) but ectodermal cells are stretched across the urethral lumen ventrally (arrowhead). (I-L) Coronal histological sections reveal a conical urethral lumen (asterisks) in controls and a hypoplastic, clover-shaped lumen in $Fgfr2^{Ecto\Delta}$ urethrae. NFR, Nuclear Fast Red. Scale bars: 50 µm.

dorsal to ventral; the urethral lumen was larger in the dorsal side than in the ventral side of the genital tubercle (Fig. 4I,J). By contrast, the sides of the urethral epithelium in $Fgfr2^{Ecto\Delta}$ mutants were stretched laterally, resulting in a clover-shaped tube (Fig. 4K,L). These data demonstrate that deletion of *Fgfr2* from the surface ectoderm affects two aspects of embryonic external genital anatomy: preputial swelling position and urethral tube morphology. Failure of ventral prepuce formation is associated with opening of the endodermal urethral plate (and, later, the tube) along the ventral midline, resulting in hypospadias.

Fgfr2 regulates epithelial cell shape and stratification

To better understand the nature of the epithelial defects that were observed in histological sections, we performed high-resolution transmission electron microscopy (TEM) analysis of $Fgfr2^{Endo\Delta}$ and $Fgfr2^{Ecto\Delta}$ genital tubercles at E14.5. To facilitate visualization of the epithelia, we pseudocolored cells based on their positions; those in contact with the urethral lumen (urethra) or the extraembryonic space (ectoderm) were tinted magenta, cells abutting the mesenchyme were tinted cyan and all remaining cells that contacted neither surface were tinted yellow. Control urethrae at E14.5 formed stratified epithelia of 3-6 cell layers (Fig. 5A), whereas $Fgfr2^{Endo\Delta}$ mutant urethral epithelia had 1-3 cell layers throughout the epithelial sheet (Fig. 5B). In the ectoderm of both $Fgfr2^{Ecto\Delta}$ mutants and controls, the epithelia were stratified 3-5 cell layers thick (Fig. 5C,D), suggesting that *Fgfr2* mediates epithelial stratification in the urethra only.

In control urethral and ectodermal epithelia, basal cells were columnar and elongated perpendicular to the basement membrane, intermediate cells were smaller and rounded, and apical cells were rounded or, in the urethral epithelium, squamous (Fig. 5A,C). $Fgfr2^{Endo\Delta}$ urethral cell shape was more homogenous; along the apicobasal axis, all cells were cuboidal or rounded and had no obvious orientation within the epithelial sheet (Fig. 5B). Similarly, the basal cells in the surface epithelium of $Fgfr2^{Ecto\Delta}$ mutants failed to develop a columnar morphology; in each epithelial layer, cells were flat and elongated parallel, rather than perpendicular, to the basement membrane (Fig. 5D). These data indicate that endodermal *Fgfr2* regulates epithelial stratification and basal cell morphogenesis within the urethra, and that *Fgfr2* in the ectoderm controls basal cell shape, but not stratification, in the surface epithelium.

Cytoskeletal and cell adhesion defects in *Fgfr2* conditional mutants

We next investigated the mechanisms responsible for the cellular defects that occur in the epithelia of *Fgfr2* conditional mutants. Given that epithelial organization and polarity are perturbed in both conditional mutants, we asked how *Fgfr2* deletion impacts actin dynamics and cell adhesion in $Fgfr2^{Endo\Delta}$ and $Fgfr2^{Ecto\Delta}$ epithelia. We used phalloidin staining to monitor filamentous actin and immunofluorescence for β-catenin (a required component in adherens junctions; also known as Ctnnb1 – Mouse Genome Informatics) to investigate cell adhesion. Our TEM results showed that normal basal urethral cells at E14.5 were columnar and elongated perpendicular to the basement membrane; phalloidin staining demonstrated that this organization was supported by a scaffold of actin filaments that localized to the cell cortices as long, fibrous bundles (Fig. 5E). At boundaries between adjacent basal cells, enriched F-actin staining was visible (Fig. 5E) and punctate regions of β-catenin were localized to basolateral cell margins (Fig. 5K). In $Fgfr2^{Endo\Delta}$ basal urethral cells, as in controls, actin filaments were largely oriented perpendicular to the basement membrane; however, F-actin domains were short and hatched rather than long and fibrous (Fig. 5D), and basolateral β-catenin domains were not detected (Fig. 5L), suggesting that cell shape defects occur in conjunction with cytoskeletal disorganization and diminished cell adhesion.

The ventral seam of the genital tubercle showed regional differences in phalloidin staining along the proximodistal axis. In distal planes, where the urethral plate had not yet delaminated to form a tube, we found an enrichment of elongated actin filaments at

Development (2015) 142, 2203-2212 doi:10.1242/dev.119891

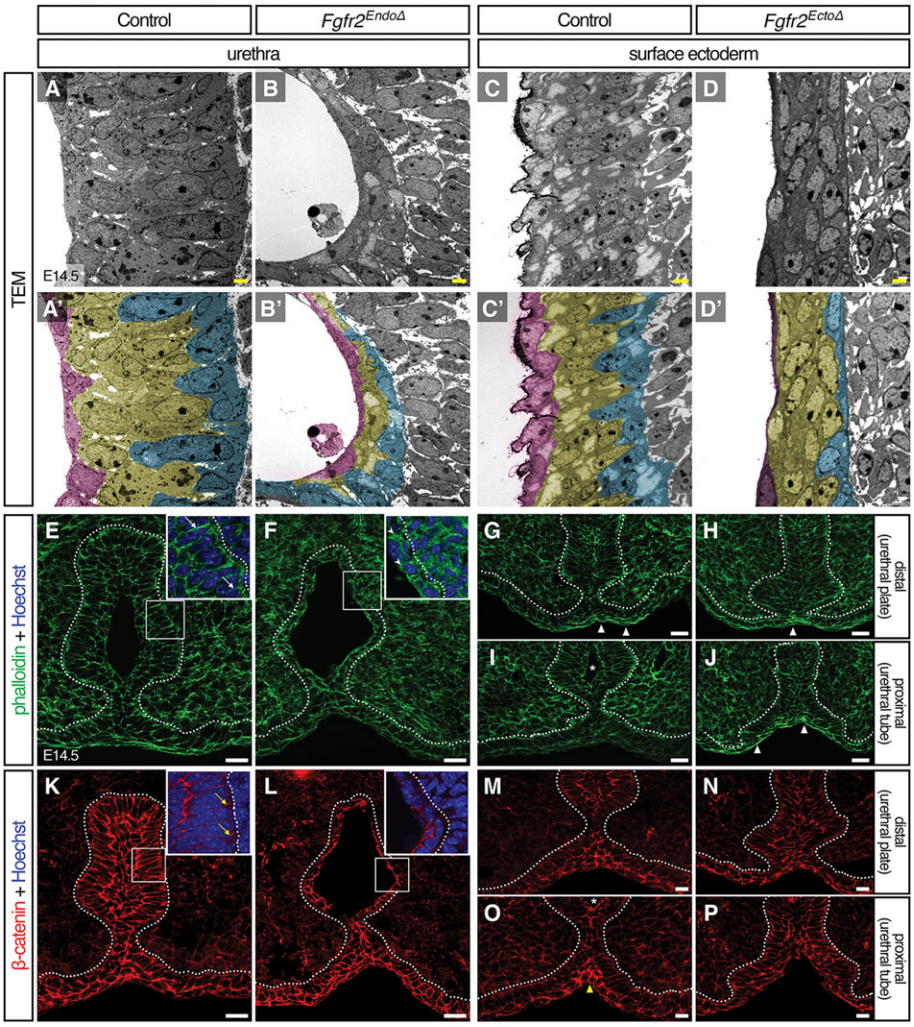

Fig. 5. Deletion of *Fgfr2* disrupts epithelial cell shape, cytoskeletal organization, and cell adhesion. (A-D′) Ultrastructural analysis by TEM reveals aberrant cell shapes in *Fgfr2*$^{-}$ genital tubercle epithelia; mutant basal cells fail to elongate perpendicular to the basement membrane in both *Fgfr2*^{EndoΔ} and *Fgfr2*^{EctoΔ} mutant epithelia. Diminished stratification is evident in the *Fgfr2*^{EndoΔ} urethra. Cells adjacent to basement membrane are pseudocolored cyan, those neighboring the lumen are magenta and intervening cells are yellow. Scale bars: 2 µm. (E-P) Fluorescent micrographs of control, *Fgfr2*^{EndoΔ} and *Fgfr2*^{EctoΔ} genital tubercles stained with phalloidin (E-J) or immunolabeled with an anti-β-catenin antibody (K-P). Note the long cell cortices stained with F-actin in E (white arrows) and short, hatched phalloidin domains in F (arrowheads). Punctate, basolateral foci of β-catenin are evident in control basal urethral cells (yellow arrows) but were not detected in *Fgfr2*^{EndoΔ} mutants. In controls, the ventral seam shows enriched actin stress fibers (white triangles) distally and increased β-catenin staining (yellow triangles) proximally. Elevated abundance of F-actin fibers is coincident with static levels of β-catenin intensity along the proximodistal ventral midline of *Fgfr2*^{EctoΔ} mutants. Asterisks mark urethral lumen, dotted lines outline the urethral and surface epithelia. Scale bars: 20 µm.

the ventral seam (Fig. 5G). Increased F-actin was absent from the ventral genital ectoderm in proximal regions where the urethra had canalized to form an open lumen (Fig. 5I), although these regions displayed locally elevated β-catenin staining (Fig. 5O). In *Fgfr2*^{EctoΔ} mutants, local enrichment of filamentous actin bundles at the ventral midline was present along the entire proximodistal axis of the genital tubercle (Fig. 5H,J), and no increases in β-catenin staining were detected at the ventral ectodermal midline (Fig. 5N,P). These data suggest that urethral canalization involves dynamic changes in cytoskeletal rigidity and adhesion at the ectodermal-endodermal boundary, and that these processes are misregulated in *Fgfr2*^{EctoΔ} mutants.

Fgfr2 controls proliferation in urethral and surface epithelia by regulating the G1/S transition

To determine whether the epithelial defects in *Fgfr2*^{EndoΔ} and *Fgfr2*^{EctoΔ} mutants include disrupted cell proliferation, we first quantified cell number in mutant versus control epithelia. Cell counting showed reduced numbers of urethral cells in *Fgfr2*^{EndoΔ} mutants, with an average of only 67 urethral cells per transverse section compared with 123 urethral cells per section in controls (P>0.001), although cell numbers in the genital mesenchyme were similar (*Fgfr2*^{EndoΔ} mesenchyme: 84 cells per 70 µm^2; control mesenchyme: 88 cells per 70 µm^2, P=0.38; Fig. 6A). Similarly, there were significantly fewer ectodermal cells per 70 µm^2 in *Fgfr2*^{EctoΔ} mutants (51 cells) compared with controls (82 cells, P>0.001; Fig. 6A). To test the hypothesis that decreased cell numbers are caused by diminished cell proliferation, we used BrdU labeling to calculate the mitotic indices of urethral epithelial cells in *Fgfr2*^{EndoΔ} mutants and of surface ectodermal cells in *Fgfr2*^{EctoΔ} mutants. We found a significantly lower mitotic index in *Fgfr2*^{EndoΔ} urethral cells (17.7%) compared with control urethral cells (34.9%, P<0.001; Fig. 6B). We also found that the mitotic index of ectodermal cells in *Fgfr2*^{EctoΔ} mutants was significantly lower (17.9%) than control ectodermal cells (24.4%, P<0.005; Fig. 6B). As a control, we monitored the mitotic indices of Cre^{-} mesenchymal cells in *Fgfr2*^{EndoΔ} mutants and controls and found no significant differences (33.4% and 34.5%, respectively; Fig. 6B). These data indicate that *Fgfr2* regulates epithelial cell proliferation in the urethra and surface ectoderm of the genital tubercle.

For insight into the mechanism by which *Fgfr2* regulates cell proliferation, we examined cell cycle kinetics of mutant cells in both *Fgfr2*^{EndoΔ} and *Fgfr2*^{EctoΔ} embryos. We calculated the lengths of G1/G0, G2/M, and S phases, as well as total cell cycle duration for individual cell populations (Seifert et al., 2010). In the urethral epithelium of control embryos, the average length of G1 was 8.1 h and total cell cycle time was 12.1 h, but in *Fgfr2*^{EndoΔ} urethral cells the average length of G1 was 25.5 h and total cell cycle time was 29.5 h (G1/S: P<0.001, total: P<0.001; Fig. 6C). We found no significant differences in the lengths of S phase and G2/M (Fig. 6C). Deletion of *Fgfr2* from ectodermal cells has a similar effect on cell cycle kinetics; in control ectodermal cells, G1 length

Development (2015) 142, 2203-2212 doi:10.1242/dev.119891

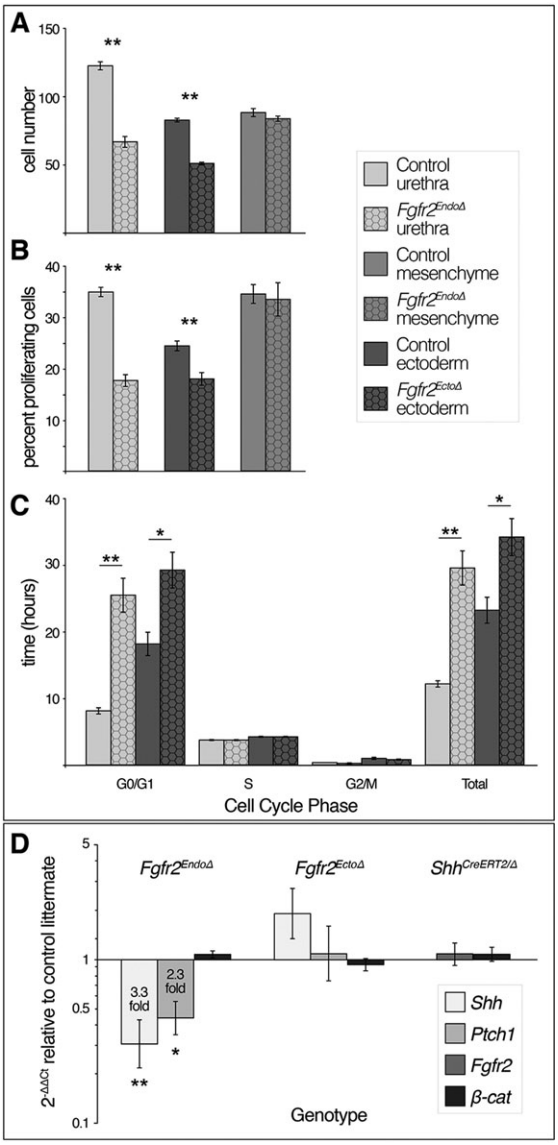

Fig. 6. *Fgfr2*-mediated cell cycle progression and genetic interactions among *Fgfr2*, *Shh* and *β-catenin* signaling. (A-C) $Fgfr2^{\Delta}$ tissue compartments of $Fgfr2^{Endo\Delta}$ and $Fgfr2^{Ecto\Delta}$ mutants have significantly fewer cells, decreased mitotic indices, longer G0/G1 phases and longer total cell cycle times relative to littermate controls. (D) qRT-PCR comparing levels of *Fgfr2*, *Shh*, *Ptch1* and *β-catenin* in tissue-specific *Fgfr2* and $Shh^{CreERT2/\Delta}$ conditional mutants relative to control littermates. Target gene expression was normalized to *Gapdh*. Error bars indicate s.d. *$P \leq 0.05$, **$P \leq 0.005$ (Student's *t*-test).

was 18.1 h and the total cell cycle time was 23.2 h. By contrast, $Fgfr2^{Ecto\Delta}$ ectodermal cells have an average G1 length of 29.1 h and total cell cycle time of 34.1 h (G1/S: $P<0.01$, total: $P=0.01$; Fig. 6C). No significant differences in the times of S and G2/M phases were detected in $Fgfr2^{Ecto\Delta}$ cells (Fig. 6C). As conditional deletion of *Fgfr2* significantly lengthens G1, and, consequently, total cell cycle time is increased, we conclude that *Fgfr2* regulates cell proliferation by promoting the G1/S transition both in the urethral epithelium and in the surface ectodermal epithelium.

Transcriptional interactions among *Fgfr2*, *Shh* and *β-catenin*

Global deletion of *Fgfr2iiib* results in a premature downregulation of *Shh* in the urethra (Petiot et al., 2005). Based on the *Shh* expression pattern and the phenotypes of tissue-specific *Fgfr2* conditional knockouts, decreased *Shh* in $Fgfr2iiib^{-/-}$ mice could be a direct consequence of endodermal *Fgfr2* deletion (meaning that *Fgfr2* mediates *Shh* in a cell-autonomous manner), an indirect effect of fewer urethral cells (due to loss of endodermal *Fgfr2*), or an indirect effect of ectodermal *Fgfr2* deletion (suggesting that *Shh* is regulated by an intermediate signal controlled by *Fgfr2* in the ectoderm). To determine the tissue-specific roles of *Fgfr2* in the regulation of *Shh* expression, we compared the levels of *Shh* mRNA in genital tubercles of $Fgfr2^{Endo\Delta}$, $Fgfr2^{Ecto\Delta}$ and control mice by quantitative real-time PCR (qRT-PCR). We also examined levels of the *Shh* target gene *Patched1* (*Ptch1*) to monitor *Shh* signal transduction. Genital tubercles of $Fgfr2^{Endo\Delta}$ mutants showed a 3.3-fold decrease in *Shh* expression ($P=0.005$) and a 2.3-fold decrease in *Ptch1* ($P=0.006$), whereas $Fgfr2^{Ecto\Delta}$ genital tubercles showed no significant differences in *Shh* or *Ptch1* expression levels (Fig. 6D). Thus, hedgehog signaling is diminished as a result of endodermal *Fgfr2* deletion but is unaffected by ectodermal *Fgfr2* deletion.

In light of our finding that endodermal *Fgfr2* deletion results in diminished *Shh* signaling, we tested whether *Fgfr2* and *Shh* function in a feedback loop during development of the external genitalia. To test this possibility, we examined the expression levels of *Fgfr2* in *Shh* mutant genital tubercles. As $Shh^{-/-}$ embryos fail to develop external genitalia beyond rudimentary paired genital swellings (Haraguchi et al., 2001; Perriton et al., 2002), we used inducible Cre [$Shh^{CreERT2}$; Harfe et al. (2004)] and floxed [Shh^{C}; Dassule et al. (2000)] alleles to conditionally delete *Shh* at E11.5, and we monitored the levels of *Fgfr2* mRNA in E14.5 genital tubercles by qRT-PCR. $Shh^{CreERT2/\Delta}$ genital tubercles showed no change in *Fgfr2* expression levels (Fig. 6D). Based on these data, we conclude that *Fgfr2* is required for normal expression of *Shh* but that *Shh* does not feed back to regulate *Fgfr2*. This is consistent with our previous report that urethral epithelial cells do not express *Ptch1* (Seifert et al., 2009), and therefore do not respond directly to *Shh*.

Conditional deletion of *β-catenin* from the urethral endoderm causes transcriptional downregulation of *Shh*, *Ptch1* and *Fgfr2* (Lin et al., 2008). Our immunohistochemical analyses demonstrated that β-catenin was mislocalized in mutant epithelia of $Fgfr2^{Endo\Delta}$ and $Fgfr2^{Ecto\Delta}$ conditional knockout mutants; to identify whether these defects were caused by changes in *β-catenin* transcription, and to determine whether *Shh* and *β-catenin* function in a feedback loop, we analyzed the levels of *β-catenin* expression in *Fgfr2* and *Shh* conditional knockout genital tubercles by qRT-PCR. We found no changes in *β-catenin* transcription levels in $Fgfr2^{Endo\Delta}$, $Fgfr2^{Ecto\Delta}$ or $Shh^{CreERT2/\Delta}$ genital tubercles as compared with control littermates (Fig. 6D). These data suggest that changes in β-catenin localization in $Fgfr2^{\Delta}$ epithelia occur at the level of the protein, and that *β-catenin* and *Shh* are not involved in a feedback loop in genital tubercle morphogenesis at E14.5.

DISCUSSION

Complete loss of *Fgfr2* from the external genital epithelia results in three major anomalies: hypospadias due to defective ventral growth of the prepuce, loss of progenitor cells in the urethral endoderm and concomitant decrease in proliferation and stratification (Petiot et al., 2005). *Fgfr2* deletion from urethral endoderm or the surface ectoderm resulted in two distinct phenotypes: endodermal *Fgfr2* ablation causes mild hypospadias with arrested development of the urethral epithelium, and loss of ectodermal *Fgfr2* induces severe hypospadias and hypoplasia of the ventral prepuce. We conclude that *Fgfr2* activity in the endoderm mediates urethral epithelial maturation, whereas ectodermal *Fgfr2* is required for formation of the prepuce. In both the urethral and the surface epithelia of

Development (2015) 142, 2203-2212 doi:10.1242/dev.119891

the genital tubercle, *Fgfr2* promotes proliferation by mediating the G1/S cell cycle transition and is required for adhesion and morphological maturation of basal epithelial cells. We found significant decreases in *Shh* and *Ptch1* upon deletion of endodermal *Fgfr2*, but it is possible that this is an indirect result of fewer urethral cells rather than a direct consequence of *Fgfr2* regulating hedgehog signaling; our finding that the mesenchymal cells of *Fgfr2* conditional mutants show no changes in proliferation support this interpretation. Our findings highlight the interdependence of urethral tubulogenesis with formation of the ventral prepuce and dimorphic patterning of the distal urethra, and suggest that structural integrity of the ectodermal-endodermal boundary at the ventral midline integrates these morphogenetic events and is regulated by Fgf signaling. Despite the distinctive phenotypes resulting from *Fgfr2* conditional deletions, our data suggest that *Fgfr2* mediates the same cellular processes in both the endoderm and the ectoderm of the developing genital tubercle.

Both endodermal and ectodermal *Fgfr2* maintain the structural integrity of the ventral seam that is required for tubulogenesis and prepuce formation

Cavitation of the bilaminar urethral plate epithelium progresses from proximal to distal, resulting in a cylindrical urethral tube (Van Der Werff et al., 2000; Hynes and Fraher, 2004; Cohn, 2011). Our finding that $Fgfr2^{Endo\Delta}$ mutants fail to develop a penile urethral lumen suggests that cavitation requires endodermal *Fgfr2* activity. We previously reported that a thin layer of ectoderm overlies the endoderm at the ventral margin of the developing urethra (Seifert et al., 2009). In $Fgfr2^{Endo\Delta}$ mutants, this boundary is not strictly maintained; an irregular border between endoderm and ectoderm, identified by lineage tracing, indicates that $Fgfr2^{\Delta}$ endodermal cells intercalate with ectodermal cells, resulting in a relaxation of lineage-restricted compartmentalization. A loss of tissue integrity due to decreased cell proliferation and epithelial maturation following *Fgfr2* deletion in the urethra disrupts lineage compartmentalization at the ventral ectodermal-endodermal boundary, and failure to form a discrete urethral epithelium covered by surface ectoderm results in exposure of the underlying urethral lumen and mislocalization of endodermal cells.

Mechanosensation of changes in environmental rigidity involve extension of actin filaments (Vogel and Sheetz, 2006). We interpret the local upregulation of actin fibers at the ventral seam of the genital tubercle as evidence of cells sensing mechanical tension, and that response to this tension involves increased cell adhesion (evidenced by increased β-catenin). The finding that actin-rich stress fibers are produced in this region of $Fgfr2^{Ecto\Delta}$ mutants suggests that the cells are able to sense increases in mechanical force; however, the absence of increased β-catenin suggests an inability of the ectodermal cells to respond to increased strain. Given the decreased proliferation in the surface epithelium of $Fgfr2^{Ecto\Delta}$ mutants, we postulate that this results in a discrepancy between the rates at which the volume and surface area of the genital tubercle increase, causing rupture of the surface epithelium and an open (hypospadic) urethra. Signs of mechanical failure are evident in $Fgfr2^{Ecto\Delta}$ external genitalia; we noted thin, damaged cellular remnants overlying the hypospadic urethra and infer that these projections are the result of a loss of epithelial contact at the endodermal-ectodermal boundary. Simultaneous loss of epithelial integrity along the ventral midline and misdirected lateral growth of the preputial swellings in $Fgfr2^{Ecto\Delta}$ mutants suggests that normal ventrolateral preputial development requires strong epithelial integrity at the ectodermal-endodermal boundary. We propose that this axis along the ventral midline of the genital tubercle acts as a scaffold around which the preputial swellings eventually fuse. Therefore, disruption of this hinge point due to mechanical stress in $Fgfr2^{Ecto\Delta}$ mutants causes lateral displacement of the preputial swellings and precludes formation of a complete prepuce.

Tissue-specific *Fgfr2* deletions disrupt distinct aspects of organogenesis via a common cellular mechanism

Coordinated cell shape changes mediate tubulogenesis of many organs (Vogel and Sheetz, 2006; Davidson, 2008; Davidson et al., 2010; Sawyer et al., 2010; Eom et al., 2011; Joshi and Davidson, 2012; Plosa et al., 2012; Caviglia and Luschnig, 2014; Girdler and Röper, 2014). Cytoskeletal reorganizations underlie cell shape changes, require cell adhesion and occur in a cell-cycle-dependent manner (Yonemura et al., 1995; Girdler and Röper, 2014). Fgf receptor activation can induce cytoskeletal rearrangement in conjunction with stimulating the G1/S transition (Steele et al., 2006), and promotes the G1/S transition in other contexts of tubulogenesis (Yin et al., 2008). We found that *Fgfr2* mediates columnar morphogenesis of basal cells and the G1/S cell cycle transition throughout the developing external genital epithelia. Our finding that $Fgfr2^{\Delta}$ basal urethral cells have decreased basolateral β-catenin and disorganized actin filaments implicates insufficient cell adhesion as a cause of aberrant epithelial morphogenesis. Together, these data raise the intriguing possibility that *Fgfr2* in the genital tubercle epithelia drives epithelial maturation by coupling proliferation with cellular morphogenesis.

Dimorphic urethral patterning requires Fgf signaling from multiple spatial domains

An important but poorly understood feature of sexually dimorphic external genital development is internalization of the male urethra (Glenister, 1954; Seifert et al., 2008). At initiation of external genital development, urethral endoderm contacts the ventral side of the genital tubercle (Glenister, 1954; Van der Meulen, 1964; Hynes and Fraher, 2004). In males, proximodistal invasion of urorectal septum mesenchyme into the genital tubercle contributes to displacement of the urethra to a central position within the glans (Glenister, 1954). It has been postulated that this remodeling is due to a reorganization of the urethral epithelium rather than apoptosis or EMT (Seifert et al., 2008). Our finding that male $Fgfr2^{Endo\Delta}$ mutants fail to separate the urethral tube from the ventral ectoderm supports this hypothesis and might result from deficient maturation of the urethral epithelium. This phenotype can be interpreted as a feminization, and our finding that the distal urethra of $Fgfr2^{Endo\Delta}$ mutants forms an epithelial cord similar to the clitoral endoderm supports this conclusion. Our observations that the distal urethra of $Fgfr2^{Endo\Delta}$ mutants fails to form a lumen and that this is associated with a disruption of urethral internalization suggest that urethral tubulogenesis and internalization are interdependent processes that each require *Fgfr2*.

Androgen-Fgf interactions and human hypospadias

Fgfr2 can be transcriptionally downregulated by treatment with the anti-androgen flutamide in a dose-dependent manner (Petiot et al., 2005). Flutamide treatment also results in hypospadias and persistence of urethral attachment to the ventral ectoderm (Seifert et al., 2008), phenotypes which closely resemble that of $Fgfr2^{Endo\Delta}$ mutants. Our data suggest that disruption of *Fgfr2* signaling in the urethral endoderm could be one mechanism by which anti-androgen exposure causes hypospadias, failed urethral internalization, and hypoplasia of the ventral prepuce. Deviation of the penoscrotal

Development (2015) 142, 2203-2212 doi:10.1242/dev.119891

raphe from the ventral midline has been demonstrated to correlate with mild hypospadias in humans (Mohan et al., 2014). The observation that deletion of *Fgfr2* from the urethral endoderm perturbs compartmentalization of the endodermal-ectodermal boundary along the ventral midline of the developing penis raises the possibility that mild hypospadias with penoscrotal raphe anomalies could result from aberrant urethral *Fgfr2* signaling.

Taken together, these results provide new insights into the cellular mechanisms that govern morphogenesis of the prepuce and internalized urethra. The endodermal and ectodermal domains of *Fgfr2* play distinct roles in urethral tubulogenesis; however, in both tissue compartments Fgfr2 controls epithelial cell proliferation, stratification and adhesion. Coordination of these cellular processes in the urethral epithelium and the overlying surface ectoderm is required both for synchronous development and for structural integrity of the developing urethral tube and prepuce.

MATERIALS AND METHODS

Transgenic embryo generation and collection

Mouse strains with the *Msx2*-Cre (Sun et al., 2000), Shh^{gfpcre} (Harfe et al., 2004), $Fgfr2^{flox}$ (Yu et al., 2003), $Rosa26^{lacZ}$ (Soriano, 1999), $Shh^{creERT2}$ (Harfe et al., 2004) and Shh^{C} (Dassule et al., 2000) transgenes have been previously described. Timed matings were generated by crossing male mice carrying Cre and one floxed allele to females homozygous for the floxed allele. Pregnant $Shh^{C/C}$ females were dosed with 10 mg/kg tamoxifen by oral gavage at E10.5 to induce recombination. Pregnant dams were euthanized by cervical dislocation; neonatal mice were anesthetized by isoflurane inhalation and euthanized by decapitation. Protocol-specific dissection and fixation parameters are listed in supplementary material Table S1. Tail biopsies were used to genotype for sex and the presence of Cre, conditional (*Fgfr2* or *Shh*), and reporter alleles by standard PCR (supplementary material Table S4).

Lineage tracing

In mice carrying the *R26R* allele, β-galactosidase activity in the external genitalia of neonates and embryos was detected by X-Gal staining according to published methods (Hogan et al., 1994).

Histology, immunohistochemistry and immunofluorescence

Preparation of tissue sections and histological stains are described in supplementary material Table S2. For colorimetric immunohistochemistry, slides were dewaxed, rehydrated, and microwaved in citrate buffer, pH 6.0 (Invitrogen) for antigen retrieval. Endogenous peroxidase activity was quenched in 2% hydrogen peroxide and nonspecific binding was inhibited with blocking solution (10% goat serum, 2% lyophilized bovine serum albumin, 0.1% Tween-20 in PBS) prior to overnight incubation in primary antibody (supplementary material Table S3). Slides were then rinsed, incubated in secondary antibody diluted in blocking solution and developed with diaminobenzidine (DAB, Thermo Scientific). Immunofluorescence was performed similarly, except that antigen retrieval and peroxidase quenching were omitted. Filamentous actin was detected by a 20-min incubation in Alexa Fluor 488-conjugated phalloidin (Molecular Probes) diluted 1:10 in PBS following removal of the secondary antibody. DNA was stained with Hoechst 33342, and slides were mounted with fluorescence mounting medium (Dako) prior to confocal imaging on a Zeiss LSM 710.

SEM

Subsequent to GA/PFA fixation, genital tubercles were rinsed in PBS, osmicated in 2% OsO_4 for 1 h, dehydrated to absolute ethanol and critical-point dried. Samples were then mounted on stubs, sputter-coated with a gold/palladium alloy and imaged on a Hitachi S-4000 FE-SEM.

TEM

Genital tubercles were dehydrated to pure acetone, resin-infiltrated in graded acetone/Spurr's epoxy resin (Ellis, 2006) to 100% resin and cured at 60°C. Thin sections were collected on formvar copper slot grids, stained with 2% uranyl acetate and Reynold's lead citrate, and imaged on a Hitachi H-7000 TEM.

Cell cycle analysis

An intraperitoneal injection of BrdU at 50 mg/kg was given to pregnant dams 2 h prior to embryo harvest and immunofluorescence was performed as above. Cell-cycle phase times were calculated according to published methods (Seifert et al., 2010) on 16 transverse sections/sample.

Quantitative real-time PCR

RNA was extracted from whole E14.5 genital tubercles (Qiagen RNeasy Plus Micro Kit) and cDNA was reverse-transcribed from 500 ng of extracted RNA (Bio-Rad iScript RT cDNA Synthesis Kit). qRT-PCR reactions (18 µl volume) were synthesized using the Bio-Rad iQ SYBR Green Supermix and measured in three technical replicates. Primers are listed in supplementary material methods. At least three biological replicates were used for each primer-embryo pair. Relative expression levels were calculated by the $2^{-\Delta\Delta CT}$ method.

Acknowledgements

We thank Dr Jennifer Fernandez, Shelby Frantz, Gabriel Daniels, Rikesh Patel, Karen Kelley, Kimberly Backer-Kelley and the UF ICBR Electron Microscopy Core for technical assistance and Dr David Ornitz for the floxed *Fgfr2* mouse line.

Competing interests

The authors declare no competing or financial interests.

Author contributions

M.L.G., A.W.S. and M.J.C. designed experiments and interpreted data; M.L.G. and A.W.S. characterized the morphologies of *Fgfr2* conditional knockout mice; M.L.G. performed the analysis of *Fgfr2* mutants; M.L.G. and M.J.C. wrote the paper.

Funding

M.L.G. is supported by a University of Florida (UF) Alumni Fellowship. This study was supported by the National Institute of Environmental Health Sciences (NIEHS) [R01-ES017099] and the Howard Hughes Medical Institute (to M.J.C.). Deposited in PMC for release after 6 months.

Supplementary material

Supplementary material available online at
http://dev.biologists.org/lookup/suppl/doi:10.1242/dev.119891/-/DC1

References

Andrew, D. J. and Ewald, A. J. (2010). Morphogenesis of epithelial tubes: insights into tube formation, elongation, and elaboration. *Dev. Biol.* **341**, 34-55.

Baskin, L. S., Himes, K., Colborn, T. and Francisco, S. (2001). Hypospadias and endocrine disruption: is there a connection? *Child. Health Rev.* **109**, 1175-1183.

Beleza-Meireles, A., Lundberg, F., Lagerstedt, K., Zhou, X., Omrani, D., Frisén, L. and Nordenskjöld, A. (2007). FGFR2, FGF8, FGF10 and BMP7 as candidate genes for hypospadias. *Eur. J. Hum. Genet.* **15**, 405-410.

Carmichael, S. L., Ma, C., Choudhry, S., Lammer, E. J., Witte, J. S. and Shaw, G. M. (2013). Hypospadias and genes related to genital tubercle and early urethral development. *J. Urol.* **190**, 1884-1892.

Caviglia, S. and Luschnig, S. (2014). Tube fusion: making connections in branched tubular networks. *Semin. Cell Dev. Biol.* **31**, 82-90.

Ching, S. T., Cunha, G. R., Baskin, L. S., Basson, M. A. and Klein, O. D. (2014). Coordinated activity of Spry1 and Spry2 is required for normal development of the external genitalia. *Dev. Biol.* **386**, 1-11.

Cohn, M. J. (2011). Development of the external genitalia: conserved and divergent mechanisms of appendage patterning. *Dev. Dyn.* **240**, 1108-1115.

Dassule, H. R., Lewis, P., Bei, M., Maas, R. and McMahon, A. P. (2000). Sonic hedgehog regulates growth and morphogenesis of the tooth. *Development* **127**, 4775-4785.

Davidson, L. A. (2008). Integrating morphogenesis with underlying mechanics and cell biology. *Curr. Top. Dev. Biol.* **81**, 113-133.

Davidson, L. A., Joshi, S. D., Kim, H. Y., von Dassow, M., Zhang, L. and Zhou, J. (2010). Emergent morphogenesis: elastic mechanics of a self-deforming tissue. *J. Biomech.* **43**, 63-70.

Ellis, A. E. (2006). Solutions to the problem of substitution of ERL 4221 for vinyl cyclohexene dioxide in Spurr low viscosity embedding formulations. *Micros. Today* **14**, 32-33.

Eom, D. S., Amarnath, S., Fogel, J. L. and Agarwala, S. (2011). Bone morphogenetic proteins regulate neural tube closure by interacting with the apicobasal polarity pathway. *Development* **138**, 3179-3188.

Geller, F., Feenstra, B., Carstensen, L., Pers, T. H., van Rooij, I. A. L. M., Körberg, I. B., Choudhry, S., Karjalainen, J. M., Schnack, T. H., Hollegaard, M. V. et al. (2014). Genome-wide association analyses identify variants in developmental genes associated with hypospadias. *Nat. Genet.* **46**, 957-963.
Girdler, G. C. and Röper, K. (2014). Controlling cell shape changes during salivary gland tube formation in Drosophila. *Semin. Cell Dev. Biol.* **31**, 74-81.
Glenister, T. W. (1954). The origin and fate of the urethral plate in man. *J. Anat.* **88**, 413-425.
Haraguchi, R., Suzuki, K., Murakami, R., Sakai, M., Kamikawa, M., Kengaku, M., Sekine, K., Kawano, H., Kato, S., Ueno, N. et al. (2000). Molecular analysis of external genitalia formation: the role of fibroblast growth factor (Fgf) genes during genital tubercle formation. *Development* **127**, 2471-2479.
Haraguchi, R., Mo, R., Hui, C.-c., Motoyama, J., Makino, S., Shiroishi, T., Gaffield, W. and Yamada, G. (2001). Unique functions of Sonic hedgehog signaling during external genitalia development. *Development* **128**, 4241-4250.
Harfe, B. D., Scherz, P. J., Nissim, S., Tian, H., McMahon, A. P. and Tabin, C. J. (2004). Evidence for an expansion-based temporal Shh gradient in specifying vertebrate digit identities. *Cell* **118**, 517-528.
Hogan, B., Beddington, R., Costantini, F. and Lacy, E. (1994). *Manipulating the Mouse Embryo: A Laboratory Manual*. Plainview, NY: Cold Spring Harbor Laboratory Press.
Hynes, P. J. and Fraher, J. P. (2004). The development of the male genitourinary system: II. The origin and formation of the urethral plate. *Br. J. Plast. Surg.* **57**, 112-121.
Joshi, S. D. and Davidson, L. A. (2012). Epithelial machines of morphogenesis and their potential application in organ assembly and tissue engineering. *Biomech. Model. Mechanobiol.* **11**, 1109-1121.
Kalfa, N., Philibert, P. and Sultan, C. (2009). Is hypospadias a genetic, endocrine or environmental disease, or still an unexplained malformation? *Int. J. Androl.* **32**, 187-197.
Kalfa, N., Philibert, P., Baskin, L. S. and Sultan, C. (2011). Hypospadias: interactions between environment and genetics. *Mol. Cell. Endocrinol.* **335**, 89-95.
Kurzrock, E. A., Baskin, L. S. and Cunha, G. R. (1999). Ontogeny of the male urethra: theory of endodermal differentiation. *Differentiation* **64**, 115-122.
Lin, C., Yin, Y., Long, F. and Ma, L. (2008). Tissue-specific requirements of β-catenin in external genitalia development. *Development* **135**, 2815-2825.
Luschnig, S. and Uv, A. (2014). Luminal matrices: an inside view on organ morphogenesis. *Exp. Cell Res.* **321**, 64-70.
Michalakis, M., Tzatzarakis, M. N., Kovatsi, L., Alegakis, A. K., Tsakalof, A. K., Heretis, I. and Tsatsakis, A. (2014). Hypospadias in offspring is associated with chronic exposure of parents to organophosphate and organochlorine pesticides. *Toxicol. Lett.* **230**, 139-145.
Mohan, A., Ashton, L. and Dalal, M. (2014). Deviation of the penoscrotal median raphe: is it a normal finding or within the spectrum of hypospadias? *Indian J. Plast. Surg.* **47**, 92-92.
Nordenvall, A. S., Frisén, L., Nordenström, A., Lichtenstein, P. and Nordenskjöld, A. (2014). Population based nationwide study of hypospadias in Sweden, 1973 to 2009: incidence and risk factors. *J. Urol.* **191**, 783-789.
Paulozzi, L. J., Erickson, J. D. and Jackson, R. J. (1997). Hypospadias trends in two US surveillance systems. *Pediatrics* **100**, 831-834.
Perriton, C. L., Powles, N., Chiang, C., Maconochie, M. K. and Cohn, M. J. (2002). Sonic hedgehog signaling from the urethral epithelium controls external genital development. *Dev. Biol.* **247**, 26-46.
Petiot, A., Perriton, C. L., Dickson, C. and Cohn, M. J. (2005). Development of the mammalian urethra is controlled by Fgfr2-IIIb. *Development* **132**, 2441-2450.
Plosa, E. J., Gooding, K. A., Zent, R. and Prince, L. S. (2012). Nonmuscle myosin II regulation of lung epithelial morphology. *Dev. Dyn.* **241**, 1770-1781.
Qiao, L., Tasian, G. E., Zhang, H., Cunha, G. R. and Baskin, L. (2011). ZEB1 is estrogen responsive in vitro in human foreskin cells and is over expressed in penile skin in patients with severe hypospadias. *J. Urol.* **185**, 1888-1893.
Ray, H. J. and Niswander, L. (2012). Mechanisms of tissue fusion during development. *Development* **139**, 1701-1711.
Satoh, Y., Haraguchi, R., Wright, T. J., Mansour, S. L., Partanen, J., Hajihosseini, M. K., Eswarakumar, V. P., Lonai, P. and Yamada, G. (2004). Regulation of external genitalia development by concerted actions of FGF ligands and FGF receptors. *Anat. Embryol.* **208**, 479-486.
Sawyer, J. M., Harrell, J. R., Shemer, G., Sullivan-Brown, J., Roh-Johnson, M. and Goldstein, B. (2010). Apical constriction: a cell shape change that can drive morphogenesis. *Dev. Biol.* **341**, 5-19.
Seifert, A. W., Harfe, B. D. and Cohn, M. J. (2008). Cell lineage analysis demonstrates an endodermal origin of the distal urethra and perineum. *Dev. Biol.* **318**, 143-152.
Seifert, A. W., Bouldin, C. M., Choi, K.-S., Harfe, B. D. and Cohn, M. J. (2009). Multiphasic and tissue-specific roles of sonic hedgehog in cloacal septation and external genitalia development. *Development* **136**, 3949-3957.
Seifert, A. W., Zheng, Z., Ormerod, B. K. and Cohn, M. J. (2010). Sonic hedgehog controls growth of external genitalia by regulating cell cycle kinetics. *Nat. Commun.* **1**, 23.
Soriano, P. (1999). Generalized lacZ expression with the ROSA26 Cre reporter strain. *Nat. Genet.* **21**, 70-71.
Steele, I. A., Edmondson, R. J., Leung, H. Y. and Davies, B. R. (2006). Ligands to FGF receptor 2-IIIb induce proliferation, motility, protection from cell death and cytoskeletal rearrangements in epithelial ovarian cancer cell lines. *Growth Factors* **24**, 45-53.
Sun, X., Lewandoski, M., Meyers, E. N., Liu, Y.-H., Maxson, R. E., Jr and Martin, G. R. (2000). Conditional inactivation of Fgf4 reveals complexity of signalling during limb bud development. *Nat. Genet.* **25**, 83-86.
Tannour-Louet, M., Han, S., Corbett, S. T., Louet, J.-F., Yatsenko, S., Meyers, L., Shaw, C. A., Kang, S.-H., Cheung, S. W. and Lamb, D. J. (2010). Identification of de novo copy number variants associated with human disorders of sexual development. *PLoS ONE* **5**, e15392.
Tannour-Louet, M., Han, S., Louet, J.-F., Zhang, B., Romero, K., Addai, J., Sahin, A., Cheung, S. W. and Lamb, D. J. (2014). Increased gene copy number of VAMP7 disrupts human male urogenital development through altered estrogen action. *Nat. Med.* **20**, 715-724.
Toppari, J., Virtanen, H. E., Main, K. M. and Skakkebaek, N. E. (2010). Cryptorchidism and hypospadias as a sign of testicular dysgenesis syndrome (TDS): environmental connection. *Birth Defects Res. A Clin. Mol. Teratol.* **88**, 910-919.
Van der Meulen, J. C. H. M. (1964). *Hypospadias*. Leiden, The Netherlands: H. E. Stenfert Kroese N.V.
Van der Werff, J. F. A., Nievelstein, R. A. J., Brands, E., Luijsterburg, A. J. M. and Vermeij-Keers, C. (2000). Normal development of the male anterior urethra. *Teratology* **61**, 172-183.
Van der Zanden, L. F. M., Van Rooij, I. A. L. M., Feitz, W. F. J., Franke, B., Knoers, N. V. A. M. and Roeleveld, N. (2012). Aetiology of hypospadias: a systematic review of genes and environment. *Hum. Reprod. Update* **18**, 260-283.
Vogel, V. and Sheetz, M. (2006). Local force and geometry sensing regulate cell functions. *Nat. Rev. Mol. Cell Biol.* **7**, 265-275.
Vottero, A., Minari, R., Viani, I., Tassi, F., Bonatti, F., Neri, T. M., Bertolini, L., Bernasconi, S. and Ghizzoni, L. (2011). Evidence for epigenetic abnormalities of the androgen receptor gene in foreskin from children with hypospadias. *J. Clin. Endocrinol. Metab.* **96**, E1953-E1962.
Wang, M.-H. and Baskin, L. S. (2008). Endocrine disruptors, genital development, and hypospadias. *J. Androl.* **29**, 499-505.
Winston, J. J., Meyer, R. E. and Emch, M. E. (2014). Geographic analysis of individual and environmental risk factors for hypospadias births. *Birth Defects Res. Clin. Mol. Teratol.* **100**, 887-894.
Yiee, J. H. and Baskin, L. S. (2010). Environmental factors in genitourinary development. *J. Urol.* **184**, 34-41.
Yin, Y., White, A. C., Huh, S.-H., Hilton, M. J., Kanazawa, H., Long, F. and Ornitz, D. M. (2008). An FGF-WNT gene regulatory network controls lung mesenchyme development. *Dev. Biol.* **319**, 426-436.
Yonemura, S., Itoh, M., Nagafuchi, A. and Tsukita, S. (1995). Cell-to-cell adherens junction formation and actin filament organization: similarities and differences between non-polarized fibroblasts and polarized epithelial cells. *J. Cell Sci.* **108**, 127-142.
Yu, K., Xu, J., Liu, Z., Sosic, D., Shao, J., Olson, E. N., Towler, D. A. and Ornitz, D. M. (2003). Conditional inactivation of FGF receptor 2 reveals an essential role for FGF signaling in the regulation of osteoblast function and bone growth. *Development* **130**, 3063-3074.
Zegers, M. M. (2014). 3D in vitro cell culture models of tube formation. *Semin. Cell Dev. Biol.* **31**, 132-140.

SUPPLEMENTARY METHODS

RNA *in situ* hybridization

Deletion of *Fgfr2* from cre-expressing regions was validated by *in situ* hybridization using a digoxigenin-labeled antisense riboprobe synthesized from linearized plasmid containing exons 9–10 of *Fgfr2* (*Fgfr2iiic-TM*, kindly provided by D. Ornitz). *Fgfr2* expression in wildtype tissue was analyzed using a riboprobe recognizing the cytoplasmic tyrosine kinase domain of FGFR2 from linearized *Fgfr2TK* plasmid (De Moerlooze et al., 2000). Whole mount *in situ* hybridization was performed according to published methods (Nieto et al., 1996) with the exceptions that Triton X-100 was replaced with Tween-20 in KTBT solution and the concentration of Triton X-100 in NTMT solution was raised from 0.1% to 1%.

Experimental design

To minimize the effects of subtle stage variation among embryos within a single litter, each mutant embryo was compared to a stage-matched control littermate of the same sex. Except where noted, only data collected from male embryos was analyzed and reported. In experiments performed on tissue sections, at least 8 non-adjacent tissue sections were examined per embryo. Analysis of multiple cellular markers (e.g., cell adhesion, cytoskeletal, and cell cycle proteins) in individual genital tubercles was carried out using single antibodies on adjacent serial sections or using multiple antibodies for co-localization on single sections. Each figure in the manuscript is representative of the totality of data.

Table S1. Embryo collection and tissue fixation

Experiment	Embryonic or neonatal tissue processed	Dissection medium	Fixative	Fixation temperature, duration
X-Gal staining of β-galactosidase	Pelvis and posterior abdomen	PBS	0.2% PFA	4°C, overnight
Immunohistochemistry/ immunofluorescence	Pelvis and posterior abdomen, hindlimbs removed	PBS	0.2% PFA	4°C, overnight
Histology	Pelvis and posterior abdomen, hindlimbs removed	PBS	4% PFA	4°C, overnight
Scanning electron microscopy	Genital tubercle with ventral body wall and proximal tail	PBS	1% GA/4% PFA	4°C, overnight
Transmission electron microscopy	Genital tubercle with ventral body wall	PBS	1% GA/4% PFA in sodium cacodylate	4°C, overnight
Whole mount *in situ* hybridization	Pelvis and posterior abdomen	DEPC PBS	4% PFA	4°C, overnight
Quantitative real-time PCR	Genital tubercle	DEPC PBS	RNAlater (Qiagen)	–20°C, indefinite

Table S2. Analyses performed on tissue sections

Protocol	Preparation and infiltration	Embedding medium	Stain
Histology	Dehydrated to absolute ethanol, permeabilized with Xylene	Paraffin (1:1 Paraplast Xtra and Plus)	Masson's trichrome (Richard Allan Scientific)
Histology on X-Gal stained tissue	Dehydrated to absolute ethanol, permeabilized with Xylene	Paraffin (1:1 Paraplast Xtra and Plus)	Nuclear fast red or Harris' Hematoxylin and 1% Eosin Y
Immunohistochemistry	Dehydrated to absolute ethanol, permeabilized with Xylene	Paraffin (1:1 Paraplast Xtra and Plus)	--
Immunofluorescence	Equilibrated with 30% sucrose	OCT (Tissue-Tek)	--
Transmission electron microscopy	Dehydrated to pure acetone, resin infiltrated in graded acetone/Spurrs epoxy resin (Ellis, 2006)	Spurrs epoxy resin	2% Uranyl acetate and Reynold's lead citrate

Table S3. Antibodies

Primary antibody	Clone or catalog number	Manufacturer	Secondary antibody	Clone or catalog number	Manufacturer
Mouse IgG_3 anti-cytokeratin14	NCL-LL002	Novacastra	Goat anti-mouse IgG, HRP conjugate	P 0447	Dako
Rabbit IgG anti-Fgfr2 (Bek)	C-17	Santa Cruz	AlexaFluor-647 goat anti-rabbit IgG	A-21244	Molecular Probes
Mouse IgG_1 anti-βcatenin	14	BD Biosciences	AlexaFluor-546 goat anti-mouse IgG_1	A-21123	Molecular Probes
Rabbit IgG anti-phospho-Histone H3	06-570	Millipore	AlexaFluor-488 goat anti-rabbit IgG	A-11008	Molecular Probes
Mouse IgG_1 anti-BrdU	G3G4	Developmental Studies Hybridoma Bank	AlexaFluor-546 goat anti-mouse IgG_1	A-21123	Molecular Probes

Table S4. Primer sequences

Primer	Type	Sequence
smcx1	Genotyping	5′-CCG-CTG-CCA-AAT-TCT-TTG-G
smc4	Genotyping	5′-TGA-AGC-TTT-TGG-CTT-TGA-G
Cre forward	Genotyping	5′-TGA-CGG-TGG-GAG-AAT-GTT-AAT
Cre reverse	Genotyping	5′-GCC-GTA-AAT-CAA-TCG-ATG-AGT
$Fgfr2^{flox}$ forward	Genotyping	5′-ATA-GGA-GCA-ACA-GGC-GG
$Fgfr2^{flox}$ reverse	Genotyping	5′-TGC-AAG-AGG-CGA-CCA-GTC-AG
Shh^{C} forward	Genotyping	5′-ATG-CTG-GCT-CGC-CTG-GCT-GTG-GAA
Shh^{C} reverse	Genotyping	5′-GAA-GAG-ATC-AAG-GCA-AGC-TCT-GGC
Rosa forward	Genotyping	5′-AAA-GTC-GCT-CTG-AGT-TGT-TAT
Rosa reverse	Genotyping	5′-GGA-GCG-GGA-GAA-ATG-GAT-ATG
LacZ reverse	Genotyping	5′-GCG-AAG-AGT-TTG-TCC-TCA-ACC
βcatenin forward	qRT-PCR	5′-GTG-CAA-TTC-CTG-AGC-TGA-CA
βcatenin reverse	qRT-PCT	5′-CTT-AAA-GAT-GGC-CAG-CAA-GC
Fgfr2 forward	qRT-PCR	5′-TCT-GGG-ACC-TCC-TTC-CAT-CTT-CTT
Fgfr2 reverse	qRT-PCR	5′-ACT-GTA-GCA-AAG-TGA-GTG-GGC-GTA
GAPDH forward	qRT-PCR	5′-CCA-AGG-TCA-TCC-ATG-ACA-ACT
GAPDH reverse	qRT-PCR	5′-ATC-ACG-CCA-CAG-CTT-TCC
Ptch1 forward	qRT-PCR	5′-TTG-TGG-AAG-CCA-CAG-AAA-ACC
Ptch1 reverse	qRT-PCR	5′-TGT-CTG-GCG-TCC-GGA-TGG-A
Shh forward	qRT-PCR	5′-ACG-GAC-CTT-CAA-GAG-CCT-TA
Shh reverse	qRT-PCR	5′-CCC-ATG-GAG-CAG-GTT-TTA-GT

SUPPLEMENTARY REFERENCES

De Moerlooze, L., Spencer-Dene, B., Revest, J.-M., Hajihosseini, M., Rosewell, I. and Dickson, C. (2000). An important role for the IIIb isoform of fibroblast growth factor receptor 2 (FGFR2) in mesenchymal-epithelial signalling during mouse organogenesis. *Development* **127**, 483-492.

Nieto, M. A., Patel, K. and Wilkinson, D. G. (1996). *In situ* hybridization analysis of chick embryos in whole mount and tissue sections. *Method Cell Biol*. **51**, 219-235.

Petiot, A., Perriton, C. L., Dickson, C. and Cohn, M. J. (2005). Development of the mammalian urethra is controlled by Fgfr2-IIIb. *Development* **132**, 2441-2450.

SUPPLEMENTARY FIGURE LEGENDS

Figure S1. Conditional inactivation of *Fgfr2* in the urethral and surface epithelia of the genital tubercle. (**A-D**) *Fgfr2* expression in the developing external genitalia (Petiot et al., 2005) was validated by *in situ* hybridization on E13.5 whole genital tubercles (A,B) and transverse sections (C,D) using an antisense riboprobe complementary to the cytoplasmic tyrosine kinase (TK) domain of *Fgfr2* (*Fgfr2TK;* De Moerlooze et al., 2000). *Fgfr2* transcription was detected on the genital tubercle surface epithelium, including the preputial swellings (arrowheads), and in the developing urethra (arrow). (C,D) In tissue sections, *Fgfr2* expression was detected in the developing corpora cavernosa (cc), preputial glands (pg), urethra, and surface epithelium. In epithelia, *Fgfr2TK* transcript was most abundant in basal layers (triangle), although mRNA was also detected in suprabasal cells (D). (**E-J'**) Deletion of *Fgfr2* from target tissues was verified by whole mount *in situ* hybridization using an RNA probe specific to the floxed region of *Fgfr2*. Expression of both *Fgfr2* isoforms was visualized; the $Fgfr2^{flox}$ loxP sites flank exons 7 (IIIa), 8 (IIIb), and 9 (IIIc) (Yu et al., 2003), and the *Fgfr2iiic-TM* riboprobe hybridizes to exons 9 and 10

(transmembrane, TM). At E12.5 *Fgfr2* expression is evident in the distal urethra (arrows) of control and $Fgfr2^{Ecto\Delta}$ mutant genital tubercles but is absent from $Fgfr2^{Endo\Delta}$ mutants. By E14.5, *Fgfr2* transcripts are detectable in the urethral and surface ectodermal (arrowheads) epithelia of controls, but are absent from the urethrae of $Fgfr2^{Endo\Delta}$ mutants and from the surface ectoderm of $Fgfr2^{Ecto\Delta}$ mutants. Restriction of *Fgfr2* expression to Cre-negative regions of the genital tubercles confirms that *Fgfr2* is deleted specifically in the cells targeted by the Cre alleles. (**K-M**) Immunofluorescence of FGFR2 reveals no changes in the localization of ectodermal FGFR2 in $Fgfr2^{Endo\Delta}$ mutants, of urethral FGFR2 in $Fgfr2^{Ecto\Delta}$ mutants, or of mesenchymal FGFR2 (yellow arrows) in either mutant. Scale bars: 100 μm.

Figure S2. Variation in hypospadias and preputial anomalies resulting from ectodermal *Fgfr2* deletion. Oversized and ectopic urethral openings in $Fgfr2^{Ecto\Delta}$ mutants at P0 can be seen in β-galactosidase-stained male (**A-D**) and female (**E**), and in unstained female (**F**) genital tubercles. Urethral tube defects range in severity from glanular (A), to coronal (B), to midshaft (C), to proximal (D) hypospadias in males. Female mutants also develop hypospadias (E,F). Arrows denote urethral meatuses; arrowheads mark preputial ectoderm. Scale bars: 100 μm.

Figure S3. Urethral cells lacking *Fgfr2* do not undergo epithelial-mesenchymal transition. Immunohistochemical analysis of K14 in transverse sections of β-galactosidase-stained $Fgfr2^{Endo\Delta}$ and control genital tubercles at E14.5 shows that endodermal cells (blue) remain

within the urethral epithelium and are not detected in the adjacent mesenchyme. Scale bars: 50 μm.

Figure S4. Development of the genital tubercle in the absence of ectodermal *Fgfr2*. Light micrographs of *Fgfr2*$^{Ecto\Delta}$ mutant and control genital tubercles from stages E13 to E16 show that *Fgfr2*$^{Ecto\Delta}$ mutants develop an ectopic proximal urethral opening (insets in A-D) that expands into an abnormally large hypospadic opening (arrows in E,F). The preputial swellings are displaced dorsally at early stages (white triangles in A-D) and fail to meet at the ventral midline at later stages (black triangles in E,F). Scale bars: 100 μm.

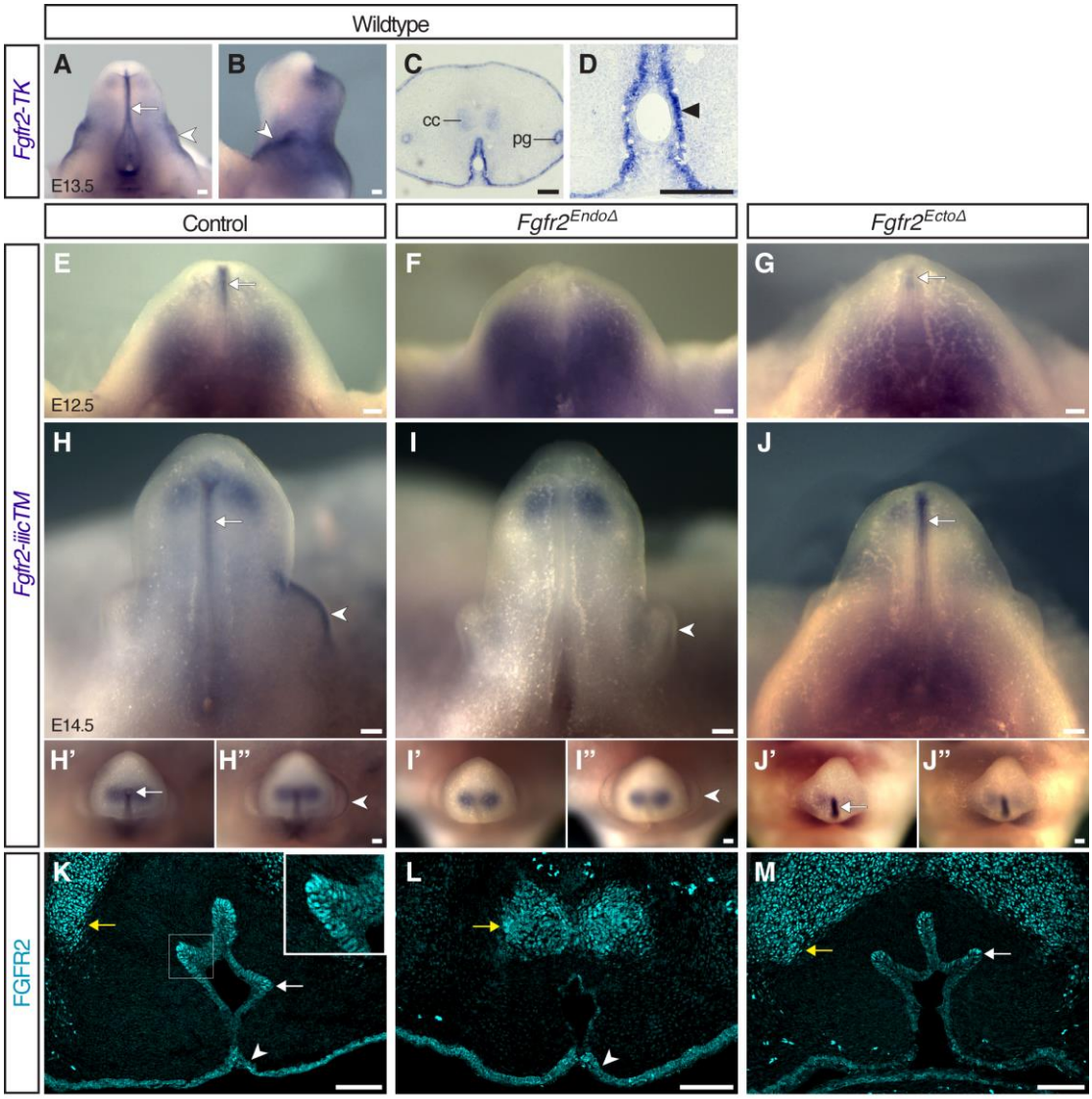

Figure S1. Conditional inactivation of *Fgfr2* in the urethral and surface epithelia of the genital tubercle.

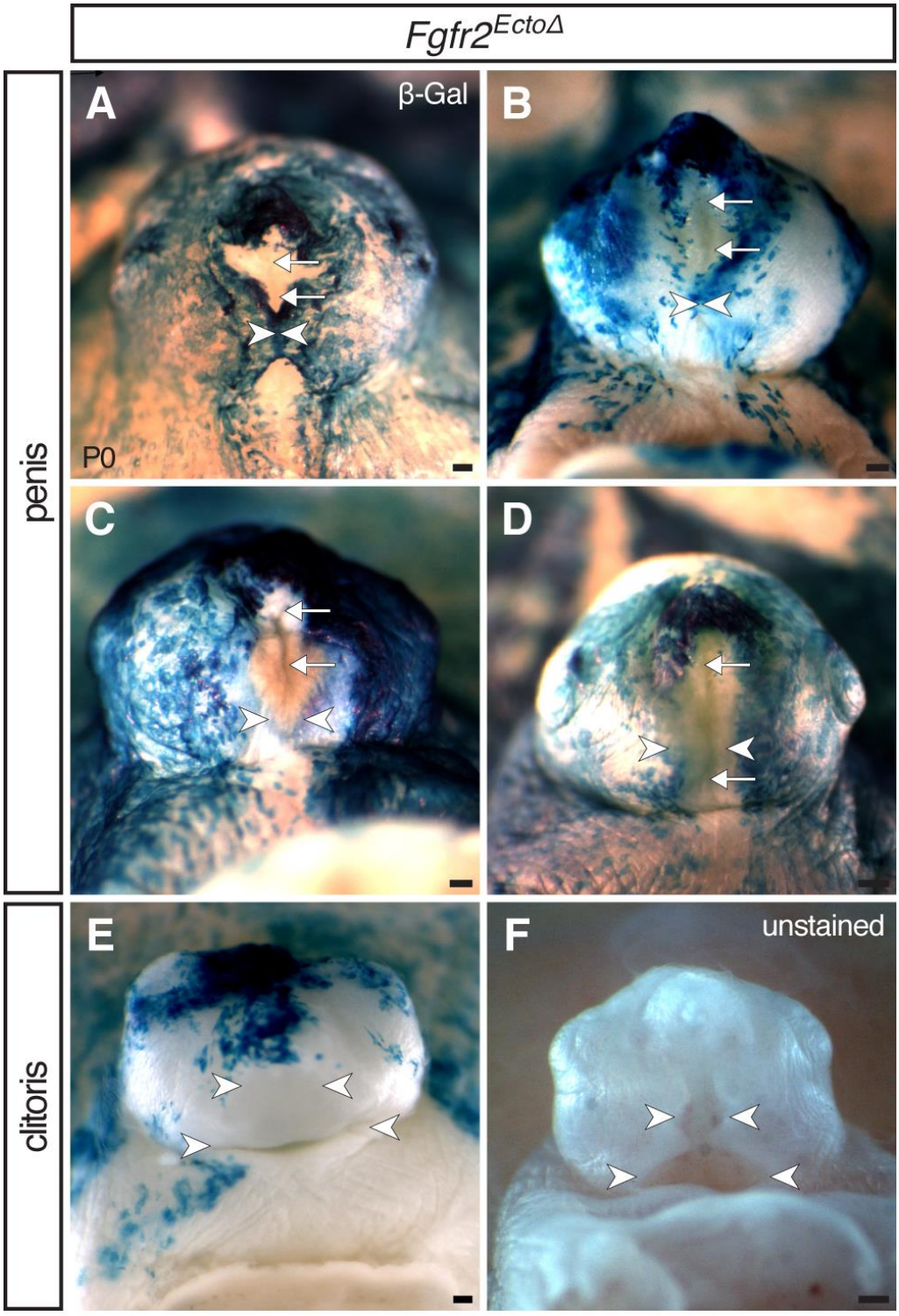

Figure S2. Variation in hypospadias and preputial anomalies resulting from ectodermal *Fgfr2* deletion.

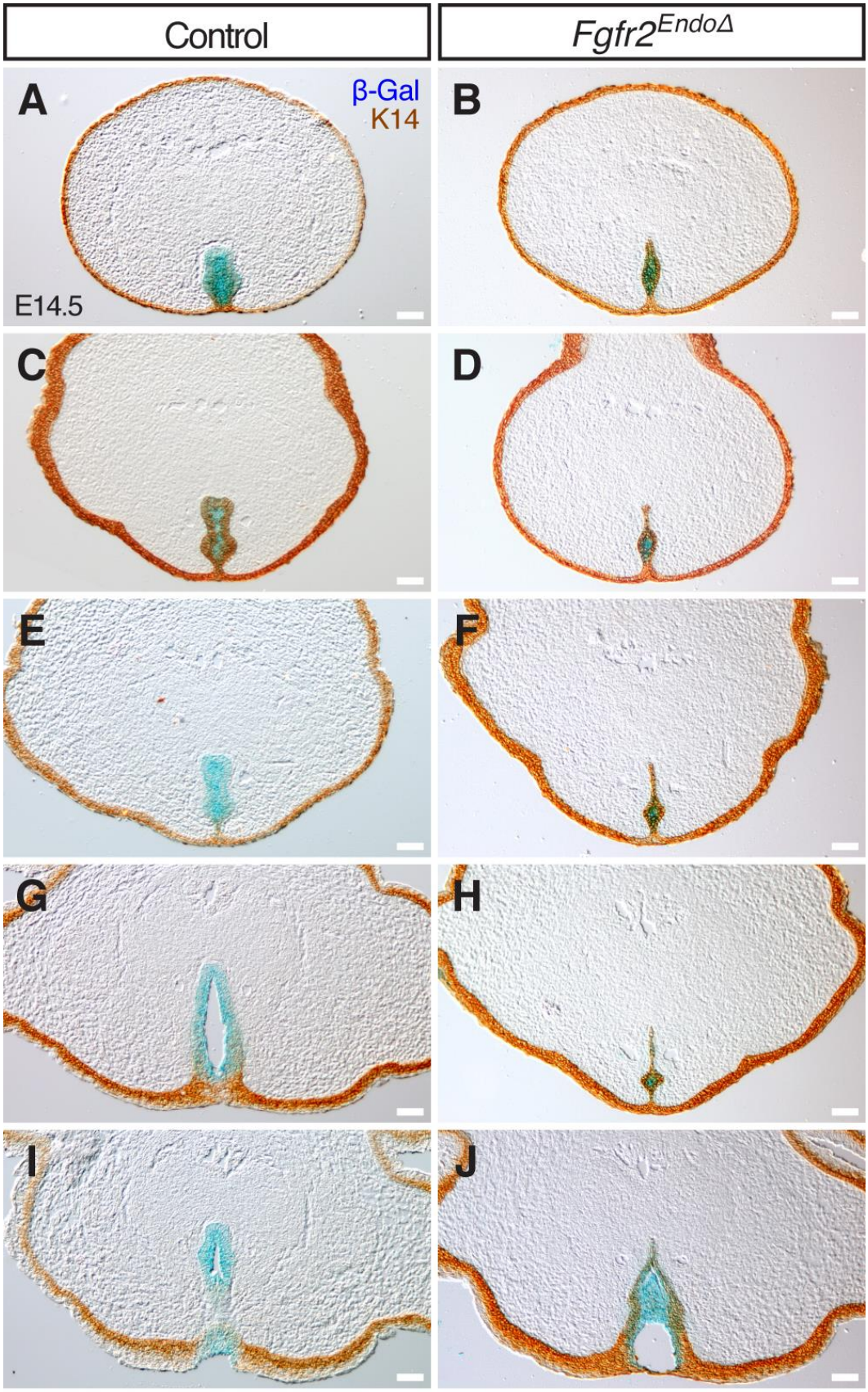

Figure S3. Urethral cells lacking *Fgfr2* do not undergo epithelial-mesenchymal transition.

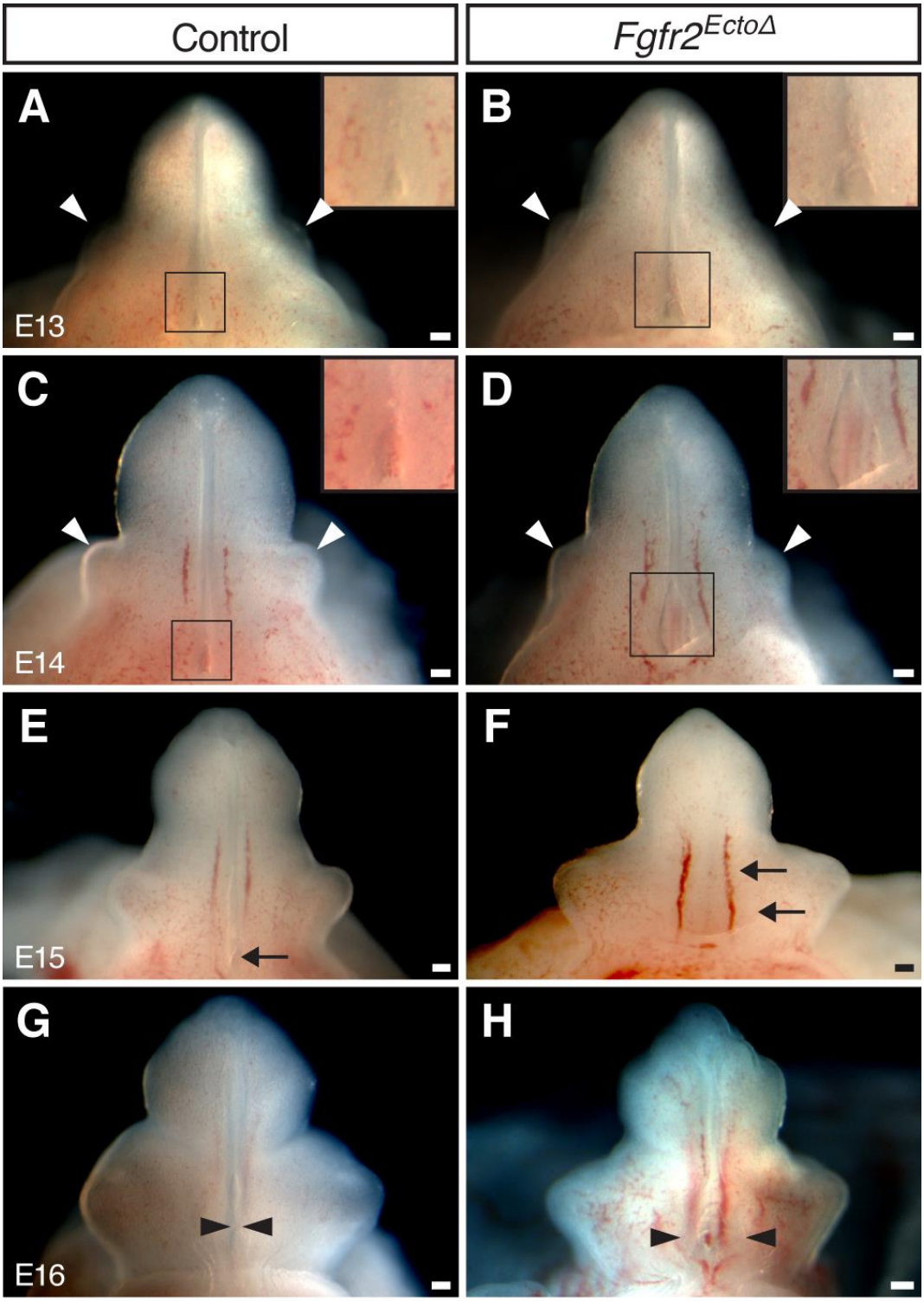

Figure S4. Development of the genital tubercle in the absence of ectodermal *Fgfr2*.